J|A|C|S ARTICLES

Published on Web 08/10/2010

Photochemical Addition of C_{60} with Siliranes: Synthesis and Characterization of Carbosilylated and Hydrosilylated C_{60} Derivatives

Junko Nagatsuka,[†] Sachie Sugitani,[†] Masahiro Kako,[‡] Tsukasa Nakahodo,[†] Naomi Mizorogi,[†] Midori O. Ishitsuka,[†] Yutaka Maeda,[§] Takahiro Tsuchiya,[†] Takeshi Akasaka,*[,†] Xingfa Gao,[||] and Shigeru Nagase[||]

Center for Tsukuba Advanced Research Alliance, University of Tsukuba, Tsukuba 305-8577, Japan, Department of Applied Physics and Chemistry, The University of Electro-Communications, Chofu 182-8585, Japan, Department of Chemistry, Tokyo Gakugei University, Koganei 184-8501, Japan, and Department of Theoretical and Computational Molecular Science, Institute for Molecular Science, Okazaki 444-8585, Japan

Received June 7, 2010; E-mail: akasaka@tara.tsukuba.ac.jp

Abstract: Photochemical reactions of C_{60} with siliranes (**1a**−**d**) afford adducts of four types (**2a**−**5b**) as carbosilylated and hydrosilylated C_{60} derivatives. Characterization of these adducts was conducted using MS, UV, NMR spectroscopy, and single-crystal X-ray analyses. In particular, the first example of the crystal structure of a closed 1,2-adduct at the 5,6-ring junction of the C_{60} cage is provided by single-crystal X-ray analysis of **3b**. Electrochemical analyses also revealed unique redox properties of the products **2b**−**5b**, which depend on the regiochemistry of the functionality, in addition to the substituents on the C_{60} cage. Theoretical calculations offer bases for the experimentally observed redox properties and relative stabilities of the silylated products.

Introduction

Much attention has been devoted to the chemical derivatization of fullerenes, which continuously yields fascinating results. Numerous studies of the fullerenes derivatized with various substituents have been reported, demonstrating applications for functionalized materials such as electronic devices.[1] To date, we have developed the functionalization of fullerenes and endohedral metallofullerenes using several reactive compounds under both thermal and photochemical conditions (Scheme 1).[2−11] We have also demonstrated that introduction

Scheme 1

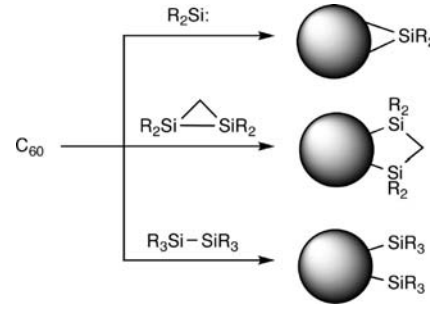

of electropositive silyl groups onto the outer surfaces of fullerenes perturbed the electronic characteristics.[2−6] For instance, the redox properties of the silylated C_{60} derivatives are changed substantially from those of C_{60} and of other C_{60}

[†] University of Tsukuba.
[‡] The University of Electro-Communications.
[§] Tokyo Gakugei University.
[||] Institute for Molecular Science.

(1) (a) Hirsch, A. *The Chemistry of the Fullerenes*; Georg Thieme Verlag: Stuttgart, 1994. (b) Taylor, R. *The Chemistry of Fullerenes*; World Scientific: Singapore, 1995. (c) Hirsch, A. *Synthesis* **1995**, 895–913. (d) Averdung, J.; Torres-Garcia, G.; Luffmann, H.; Schlachter, I.; Mattay, J. *Fullerenes, Nanotubes, Carbon Nanostructures* **1996**, *4*, 633–654. (e) Langa, F.; Nierengarten, J. F. *Fullerenes: Principles and Applications*; RSC Publishing: London, 2007. (f) Hirsch, A. *Fullerenes and Related Structures*; Springer: Berlin, 1999. (g) *Endofullerenes: A New Family of Carbon Clusters*; Akasaka, T., Nagase, S., Eds.; Kluwer: Dordrecht, The Netherlands, 2002. (h) Wakahara, T.; Kako, M.; Maeda, Y.; Akasaka, T.; Kobayashi, K.; Nagase, S. *Curr. Org. Chem.* **2003**, *7*, 927–943. (i) Martin, N. *Chem. Commun.* **2006**, 2093–2104. (j) Dunsch, L.; Yang, S. *Phys. Chem. Chem. Phys.* **2007**, *46*, 881–891. (k) Dunsch, L.; Yang, S. *Small* **2007**, *3*, 1298–1320. (l) Chaur, M. N.; Melin, F.; Ortiz, A. L.; Echegoyen, L. *Angew. Chem., Int. Ed.* **2009**, *48*, 7514–7538. (m) Tan, Y.-Z.; Xie, S.-Y.; Huang, R.-B.; Zheng, L.-S. *Nat. Chem.* **2009**, *1*, 450–460. (n) Yamada, M.; Akasaka, T.; Nagase, S. *Acc. Chem. Res.* **2010**, *43*, 92–102.

(2) (a) Akasaka, T.; Ando, W.; Kobayashi, K.; Nagase, S. *J. Am. Chem. Soc.* **1993**, *115*, 1605–1606. (b) Akasaka, T.; Mitsuhida, E.; Ando, W.; Kobayashi, K.; Nagase, S. *J. Chem. Soc., Chem. Commun.* **1995**, 1529–1530.

(3) (a) Akasaka, T.; Ando, W.; Kobayashi, K.; Nagase, S. *J. Am. Chem. Soc.* **1993**, *115*, 10366–10367. (b) Suzuki, T.; Maruyama, Y.; Akasaka, T.; Ando, W.; Kobayashi, K.; Nagase, S. *J. Am. Chem. Soc.* **1994**, *116*, 1359–1363. (c) Akasaka, T.; Mitsuhida, E.; Ando, W.; Kobayashi, K.; Nagase, S. *J. Am. Chem. Soc.* **1994**, *116*, 2627–2628. (d) Akasaka, T.; Maeda, Y.; Wakahara, T.; Okamura, M.; Fujitsuka, M.; Ito, O.; Kobayashi, K.; Nagase, S.; Kako, M.; Nakadaira, Y.; Horn, E. *Org. Lett.* **1999**, *1*, 1509–1512. (e) Maeda, Y.; Takahashi, S.; Wakahara, T.; Akasaka, T.; Sasaki, Y.; Fujitsuka, M.; Ito, O.; Kobayashi, K.; Nagase, S.; Kako, M.; Nakadaira, Y. *ITE Lett.* **2000**, *1*, 408–411. (f) Maeda, Y.; Sato, R.; Wakahara, T.; Okamura, M.; Akasaka, T.; Fujitsuka, M.; Ito, O.; Kobayashi, K.; Nagase, S.; Kako, M.; Nakadaira, Y.; Horn, E. *J. Organomet. Chem.* **2000**, *611*, 414–419.

 10.1021/ja1049719

derivatives functionalized with carbon-containing or oxygen-containing groups.[3] Moreover, results show that the circular motion of metal atoms inside the endohedral metallofullerenes is controllable by exohedral functionalization through the addition reactions of disiliranes[7] and carbenes,[8] the Bingel reaction,[9] and the Prato reaction.[10] Such regulation of encapsulated atoms is expected to be valuable for application of metallofullerenes as functional electronic and magnetic devices. However, the substrates used for silylation of fullerenes have been hitherto limited to silylenes,[2] disiliranes,[3,4] disilanes,[5] and silyl anions[12] to produce monosilylated and multisilylated derivatives. As a part of our continuing research into the chemistry of fullerenes, we conducted photoreactions of C_{60} with siliranes (silacyclopropanes), which are members of the most fundamental cyclic orgnosilanes. It has been well documented that siliranes are reactive toward various nucleophilic reagents because of their strained, polar C−Si bonds in silirane rings.[13] Recent studies have demonstrated that siliranes are useful and versatile substrates for regioselective and stereoselective syntheses.[14] If it is possible to derivatize fullerenes with activated C−Si bonds of siliranes instead of disiliranes, then novel carbosilylation reactions will be realized to fine-tune the electronic properties of fullerene derivatives.

Herein, we report the photoreactions of C_{60} with siliranes **1a**−**d** (Chart 1), describing the first example of carbosilylation of C_{60} to afford several adducts of C_{60}. In addition, we present

(4) (a) Akasaka, T.; Suzuki, T.; Maeda, Y.; Ara, M.; Wakahara, T.; Kobayashi, K.; Nagase, S.; Kako, M.; Nakadaira, Y.; Fujitsuka, M.; Ito, O. *J. Org. Chem.* **1999**, *64*, 566–569. (b) Fujitsuka, M.; Ito, O.; Maeda, Y.; Kako, M.; Wakahara, T.; Akasaka, T. *Phys. Chem. Chem. Phys.* **1999**, *1*, 3527–3531. (c) Wakahara, T.; Kondo, T.; Okamura, M.; Akasaka, T.; Hamada, Y.; Suzuki, T.; Kako, M.; Nakadaira, Y. *J. Organomet. Chem.* **2000**, *611*, 78–84. (d) Wakahara, T.; Rahman, G. M. A.; Maeda, Y.; Kako, M.; Sato, S.; Okamura, M.; Akasaka, T.; Kobayashi, K.; Nagase, S. *ITE Lett.* **2003**, *4*, 67–73. (e) Wakahara, T.; Maeda, Y.; Kako, M.; Akasaka, T.; Kobayashi, K.; Nagase, S. *J. Organomet. Chem.* **2003**, *685*, 177–188. (f) Maeda, Y.; Rahman, G. M. A.; Wakahara, T.; Kako, M.; Okamura, M.; Sato, S.; Akasaka, T.; Kobayashi, K.; Nagase, S. *J. Org. Chem.* **2003**, *68*, 6791–6794.

(5) (a) Sasaki, Y.; Konishi, T.; Fujitsuka, M.; Ito, O.; Maeda, Y.; Wakahara, T.; Akasaka, T.; Kako, M.; Nakadaira, Y. *J. Organomet. Chem.* **2000**, *599*, 216–220. (b) Sasaki, Y.; Fujitsuka, M.; Ito, O.; Maeda, Y.; Wakahara, T.; Akasaka, T.; Kobayashi, K.; Nagase, S.; Kako, M.; Nakadaira, Y. *Heterocycles* **2001**, *54*, 777–787.

(6) (a) Han, A.; Wakahara, T.; Maeda, Y.; Niino, Y.; Akasaka, T.; Yamamoto, K.; Kako, M.; Nakadaira, Y.; Kobayashi, K.; Nagase, S. *Chem. Lett.* **2001**, 974–975. (b) Wakahara, T.; Han, A.; Maeda, Y.; Niino, Y.; Akasaka, T.; Yamamoto, K.; Kako, M.; Nakadaira, Y.; Kobayashi, K.; Nagase, S. *ITE Lett.* **2001**, *2*, 649–653. (c) Wakahara, T.; Han, A.; Niino, Y.; Maeda, Y.; Akasaka, T.; Suzuki, T.; Yamamoto, K.; Kako, M.; Nakadaira, Y.; Kobayashi, K.; Nagase, S. *J. Mater. Chem.* **2002**, *12*, 2061–2064.

(7) (a) Akasaka, T.; Kato, T.; Kobayashi, K.; Nagase, S.; Yamamoto, K.; Funasaka, H.; Takahashi, T. *Nature* **1995**, *374*, 600–601. (b) Akasaka, T.; Nagase, S.; Kobayashi, T.; Suzuki, T.; Kato, K.; Yamamoto, H.; Funasaka, T.; Takahashi, T. *J. Chem. Soc., Chem. Commun.* **1995**, 1343–1344. (c) Akasaka, T.; Nagase, S.; Kobayashi, K.; Suzuki, T.; Kato, T.; Kikuchi, K.; Achiba, Y.; Yamamoto, K.; Funasaka, H.; Takahashi, T. *Angew. Chem., Int. Ed. Engl.* **1995**, *34*, 2139–2141. (d) Wakahara, T.; Matsunaga, Y.; Katayama, A.; Maeda, Y.; Kako, M.; Akasaka, T.; Okamura, M.; Kato, T.; Choe, Y.-K.; Kobayashi, K.; Nagase, S.; Huang, H.; Ata, M. *Chem. Commun.* **2003**, 2940–2941. (e) Yamada, M.; Feng, L.; Wakahara, T.; Tsuchiya, T.; Maeda, Y.; Lian, Y.; Kako, M.; Akasaka, T.; Kato, T.; Kobayashi, K.; Nagase, S. *J. Phys. Chem. B* **2005**, *109*, 6049–6051. (f) Maeda, Y.; Miyashita, J.; Hasegawa, T.; Wakahara, T.; Tsuchiya, T.; Feng, L.; Lian, Y.; Akasaka, T.; Kobayashi, K.; Nagase, S.; Kako, M.; Yamamoto, K.; Kadish, K. M. *J. Am. Chem. Soc.* **2005**, *127*, 2143–2146. (g) Wakahara, T.; Iiduka, Y.; Ikenaga, O.; Nakahodo, T.; Sakuraba, A.; Tsuchiya, T.; Maeda, Y.; Kako, M.; Akasaka, T.; Yoza, K.; Horn, E.; Mizorogi, N.; Nagase, S. *J. Am. Chem. Soc.* **2006**, *128*, 9919–9925. (h) Yamada, M.; Nakahodo, T.; Wakahara, T.; Tsuchiya, T.; Maeda, Y.; Akasaka, T.; Kako, M.; Yoza, K.; Horn, E.; Mizorogi, N.; Kobayashi, K.; Nagase, S. *J. Am. Chem. Soc.* **2005**, *127*, 14570–14571. (i) Wakahara, T.; Yamada, M.; Takahashi, S.; Nakahodo, T.; Tsuchiya, T.; Maeda, Y.; Akasaka, T.; Kako, M.; Yoza, K.; Horn, E.; Mizorogi, N.; Nagase, S. *Chem. Commun.* **2007**, 2680–2682. (j) Yamada, M.; Wakahara, T.; Tsuchiya, T.; Maeda, Y.; Kako, M.; Akasaka, T.; Yoza, K.; Horn, E.; Mizorogi, N.; Nagase, S. *Chem. Commun.* **2008**, 558–560.

(8) (a) Suzuki, T.; Maruyama, Y.; Kato, T.; Akasaka, T.; Kobayashi, K.; Nagase, S.; Yamamoto, K.; Funasaka, H.; Takahashi, T. *J. Am. Chem. Soc.* **1995**, *117*, 9606–9607. (b) Maeda, Y.; et al. *J. Am. Chem. Soc.* **2004**, *126*, 6858–6859. (c) Iiduka, Y.; Wakahara, T.; Nakahodo, T.; Tsuchiya, T.; Sakuraba, A.; Maeda, Y.; Akasaka, T.; Yoza, K.; Horn, E.; Kato, T.; Liu, M. T. H.; Mizorogi, N.; Kobayashi, K.; Nagase, S. *J. Am. Chem. Soc.* **2005**, *127*, 12500–12501. (d) Matsunaga, Y.; Maeda, Y.; Wakahara, T.; Tsuchiya, T.; Ishitsuka, M. O.; Akasaka, T.; Mizorogi, N.; Kobayashi, K.; Nagase, S.; Kadish, K. M. *ITE Lett.* **2006**, *7*, 43–49. (e) Iiduka, Y.; Wakahara, T.; Nakajima, K.; Nakahodo, T.; Tsuchiya, T.; Maeda, Y.; Akasaka, T.; Yoza, K.; Liu, M. T. H.; Mizorogi, N.; Nagase, S. *Angew. Chem., Int. Ed.* **2007**, *46*, 5562–5564. (f) Akasaka, T.; Kono, T.; Matsunaga, Y.; Wakahara, T.; Nakahodo, T.; Ishitsuka, M. O.; Maeda, Y.; Tsuchiya, T.; Kato, T.; Liu, M. T. H.; Mizorogi, N.; Slanina, Z.; Nagase, S. *J. Phys. Chem. A* **2008**, *112*, 1294–1297. (g) Tsuchiya, T.; et al. *J. Am. Chem. Soc.* **2008**, *130*, 450–451. (h) Lu, X.; Nikawa, H.; Tsuchiya, T.; Maeda, Y.; Ishitsuka, M. O.; Akasaka, T.; Toki, M.; Sawa, H.; Slanina, Z.; Mizorogi, N.; Nagase, S. *Angew. Chem., Int. Ed.* **2008**, *47*, 8642–8645. (i) Cao, B.; Nikawa, H.; Nakahodo, T.; Tsuchiya, T.; Maeda, Y.; Akasaka, T.; Sawa, H.; Slanina, Z.; Mizorogi, N.; Nagase, S. *J. Am. Chem. Soc.* **2008**, *130*, 983–989. (j) Yamada, M.; Someya, C.; Wakahara, T.; Tsuchiya, T.; Maeda, Y.; Akasaka, T.; Yoza, K.; Horn, E.; Mizorogi, N.; Nagase, S. *J. Am. Chem. Soc.* **2008**, *130*, 1171–1176. (k) Lu, X.; Nikawa, H.; Nakahodo, T.; Tsuchiya, T.; Ishitsuka, M. O.; Maeda, Y.; Akasaka, T.; Toki, M.; Sawa, H.; Slanina, Z.; Mizorogi, N.; Nagase, S. *J. Am. Chem. Soc.* **2008**, *130*, 9129–9136. (l) Akasaka, T.; et al. *J. Am. Chem. Soc.* **2008**, *130*, 12840–12841. (m) Takano, Y.; Aoyagi, M.; Yamada, M.; Nikawa, H.; Slanina, Z.; Mizorogi, N.; Ishitsuka, M. O.; Tsuchiya, T.; Maeda, Y.; Akasaka, T.; Kato, T.; Nagase, S. *J. Am. Chem. Soc.* **2009**, *131*, 9340–9346. (n) Lu, X.; Nikawa, H.; Feng, L.; Tsuchiya, T.; Maeda, Y.; Akasaka, T.; Mizorogi, N.; Slanina, Z.; Nagase, S. *J. Am. Chem. Soc.* **2009**, *131*, 12066–12067.

(9) (a) Feng, L.; Nakahodo, T.; Wakahara, T.; Tsuchiya, T.; Maeda, Y.; Akasaka, T.; Kato, T.; Horn, E.; Yoza, K.; Mizorogi, N.; Nagase, S. *J. Am. Chem. Soc.* **2005**, *127*, 17136–17137. (b) Feng, L.; Wakahara, T.; Nakahodo, T.; Tsuchiya, T.; Piao, Q.; Maeda, Y.; Lian, Y.; Akasaka, T.; Horn, E.; Yoza, K.; Kato, T.; Mizorogi, N.; Nagase, S. *Chem.—Eur. J.* **2006**, *12*, 5578–5586. (c) Feng, L.; Tsuchiya, T.; Wakahara, T.; Nakahodo, T.; Piao, Q.; Maeda, Y.; Akasaka, T.; Kato, T.; Yoza, K.; Horn, E.; Mizorogi, N.; Nagase, S. *J. Am. Chem. Soc.* **2006**, *128*, 5990–5991.

(10) (a) Cao, B.; Wakahara, T.; Maeda, Y.; Han, A.; Akasaka, T.; Kato, T.; Kobayashi, K.; Nagase, S. *Chem.—Eur. J.* **2004**, *10*, 716–720. (b) Yamada, M.; Wakahara, T.; Nakahodo, T.; Tsuchiya, T.; Maeda, Y.; Akasaka, T.; Yoza, K.; Horn, E.; Mizorogi, N.; Nagase, S. *J. Am. Chem. Soc.* **2006**, *128*, 1402–1403. (c) Yamada, M.; Okamura, M.; Sato, S.; Someya, C. I.; Mizorogi, N.; Tsuchiya, T.; Akasaka, T.; Kato, T.; Nagase, S. *Chem.—Eur. J.* **2009**, *15*, 10533–10542.

(11) (a) Maeda, Y.; Miyashita, J.; Hasegawa, T.; Wakahara, T.; Tsuchiya, T.; Nakahodo, T.; Akasaka, T.; Mizorogi, N.; Kobayashi, K.; Nagase, S.; Kato, T.; Ban, N.; Nakajima, H.; Watanabe, Y. *J. Am. Chem. Soc.* **2005**, *127*, 12190–12191. (b) Takano, Y.; Yomogida, A.; Nikawa, H.; Yamada, M.; Wakahara, T.; Tsuchiya, T.; Ishitsuka, M. O.; Maeda, Y.; Akasaka, T.; Kato, T.; Slanina, Z.; Mizorogi, N.; Nagase, S. *J. Am. Chem. Soc.* **2008**, *130*, 16224–16230. (c) Nikawa, H.; Yamada, T.; Cao, B.; Mizorogi, N.; Slanina, Z.; Tsuchiya, T.; Akasaka, T.; Yoza, K.; Nagase, S. *J. Am. Chem. Soc.* **2009**, *131*, 10950–10954. (d) Maeda, Y.; Sato, S.; Inada, K.; Nikawa, H.; Yamada, M.; Mizorogi, N.; Hasegawa, T.; Tsuchiya, T.; Akasaka, T.; Kato, T.; Slanina, Z.; Nagase, S. *Chem.—Eur. J.* **2010**, *16*, 2193–2197. (e) Lu, X.; Nikawa, H.; Tsuchiya, T.; Akasaka, T.; Toki, M.; Sawa, H.; Mizorogi, N.; Nagase, S. *Angew. Chem., Int. Ed.* **2010**, *49*, 594–597.

(12) (a) Kusukawa, T.; Ando, W. *Angew. Chem., Int. Ed. Engl.* **1996**, *35*, 1315–1317. (b) Kusukawa, T.; Ando, W. *J. Organomet. Chem.* **1998**, *561*, 109–120.

(13) (a) Seyferth, D.; Duncan, P.; Vick, S. C. *J. Organomet. Chem.* **1977**, *125*, C5–C10. (b) Seyferth, D.; Duncan, P.; Shannon, M. L. *Organometallics* **1984**, *3*, 579–583. (c) Tortorelli, V. J.; Jones, M., Jr.; Wu, S.-H.; Li, Z.-H. *Organometallics* **1983**, *2*, 759–764.

Chart 1

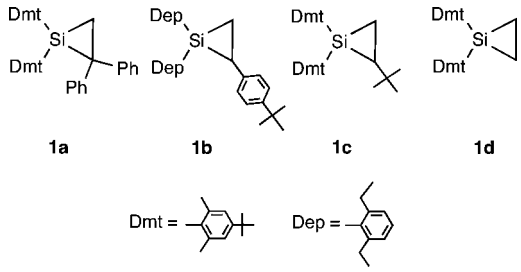

Chart 2. Possible Structures for 1,2-Adducts of C_{60} with Bridging Group X

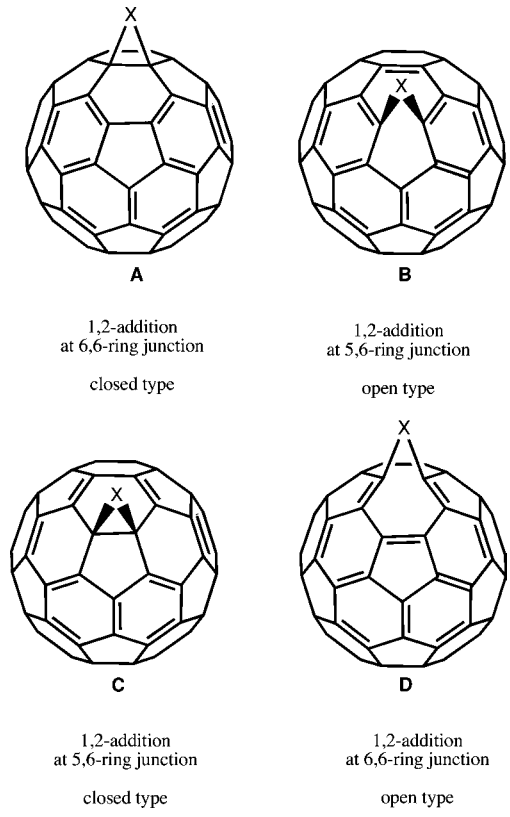

a detailed characterization of the silylated products using NMR, UV spectroscopy, mass spectrometry, cyclic voltammetry, differential pulse voltammetry, and single-crystal X-ray structural analyses along with theoretical calculations. Of particular interest is the isolation of a closed type of 1,2-adduct at the 5,6-ring junction in these reactions. There are four possible isomeric structures **A**−**D** for derivatized C_{60} resulting from 1,2-addition of various reagents, as shown in Chart 2. However, almost all reported 1,2-adducts are categorized into types **A** and **B**. Recent theoretical investigations have postulated that the production of types **C** and **D** is unfavorable because of the formation of destabilizing double bonds in five-membered rings.[15] To our knowledge, only one example of the formation of a type **C** isomer has been reported, that by Kabe et al. Nevertheless, no structural analysis using X-ray crystallography has been provided.[16] In this report, we present the first full characterization of the silylated C_{60} of the type **C**, as well as the derivatives of other addition types.

Table 1. Oxidation Potentials (E^{ox})[a] of Siliranes

	compound				
	1a	**1b**	**1c**	**1d**	**6**
E^{ox} (V)	0.22	0.47	0.84	1.17	0.24

[a] Versus ferrocene/ferrocenium couple.

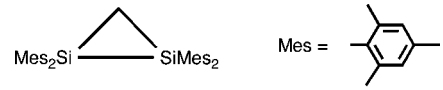

6

Results and Discussion

Photoreactions of C_{60} and Siliranes. Siliranes **1a**−**d** were synthesized using reactions of organic silylenes (Dmt_2Si: and Dep_2Si:)[17] with ethylene and substituted olefins. The oxidation potentials (E^{ox}) of **1a**−**d** are presented in Table 1, which shows that **1a** and **1b** have fairly low E^{ox} values comparable with that of disilirane **6**, whereas those of **1c** and **1d** are somewhat higher. Because **1a** and **1b** contain benzylsilane structures in their molecules, such low E^{ox} values are reasonable because of the possible $\sigma-\pi$ interaction between the ring Si−C bonds and the aryl groups attached to the ring carbon atoms. Therefore, **1a** and **1b** are expected to react readily with C_{60}, a weak electron acceptor, because it has been suggested that donor−acceptor interaction plays an important role in the photoreaction of C_{60} and **6**.[3]

Photoreactions of C_{60} with siliranes were conducted as follows. A toluene solution of **1a** and C_{60} was irradiated for 3 h with two 500-W tungsten-halogen lamps using an aqueous sodium nitrite filter solution (cutoff <400 nm) under an Ar atmosphere. After consumption of **1a**, careful separation of the reaction mixture using HPLC afforded two products, **2a** and **5a**, as shown in Scheme 2. In a similar procedure, the reaction of C_{60} and **1b** produced four adducts: **2b**, **3b**, **4b**, and **5b**. On the other hand, the photoreactions of **1c** and **1d** proceeded quite slowly, as anticipated. Irradiation of C_{60} with **1c** and **1d** for 60 h resulted in the formation of **2c** and **2d**, respectively, in lower yields, although substantial amounts of **1c** and **1d** were recovered. The structures of these products were determined using NMR, UV spectroscopy, mass spectrometry, and single-crystal X-ray structural analyses (*vide infra*). To the best of our knowledge, these results constitute the first example of carbosilylation of fullerenes.

(14) (a) Franz, A. K.; Woerpel, K. A. *Acc. Chem. Res.* **2000**, *33*, 813–820. (b) Clark, T. B.; Woerpel, K. A. *J. Am. Chem. Soc.* **2004**, *126*, 9522–9523. (c) Calad, S. A.; Woerpel, K. A. *J. Am. Chem. Soc.* **2005**, *127*, 2046–2047.

(15) (a) Prato, M.; Li, Q. C.; Wudl, F.; Lucchini, V. *J. Am. Chem. Soc.* **1993**, *115*, 1148–1150. (b) Prato, M.; Lucchini, V.; Maggini, M.; Stimpfl, E.; Scorrano, G.; Elermann, M.; Suzuki, T.; Wudl, F. *J. Am. Chem. Soc.* **1993**, *115*, 8479–8580. (c) Raghavachari, K. *Chem. Phys. Lett.* **1992**, *195*, 221–224. (d) Raghavachari, K.; Sosa, C. *Chem. Phys. Lett.* **1993**, *209*, 223–228. (e) Haddon, R. C.; Raghavachari, K. *Tetrahedron* **1996**, *52*, 5207–5220. (f) Diederich, F.; Isaacs, L.; Philp, D. *J. Chem. Soc., Perkin Trans. 2* **1994**, 391–394. (g) Wallenborn, E.-U.; Haldimann, R. F.; Klärner, F.-G.; Diederich, F. *Chem.—Eur. J.* **1998**, *4*, 2258–2265. (h) Shen, C. K.-F.; Yu, H.-H.; Juo, C.-G.; Chien, K.-M.; Her, G.-R.; Luh, T.-Y. *Chem.—Eur. J.* **1997**, *3*, 744–748.

(16) Kabe, Y.; Ohgaki, H.; Yamagaki, T.; Nakanishi, H.; Ando, W. *J. Organomet. Chem.* **2001**, *636*, 82–90.

(17) "Dmt" and "Dep" are used hereafter as abbreviations of, respectively, 4-*tert*-butyl-2,6-dimethylphenyl and 2,6-diethylphenyl groups.

Scheme 2

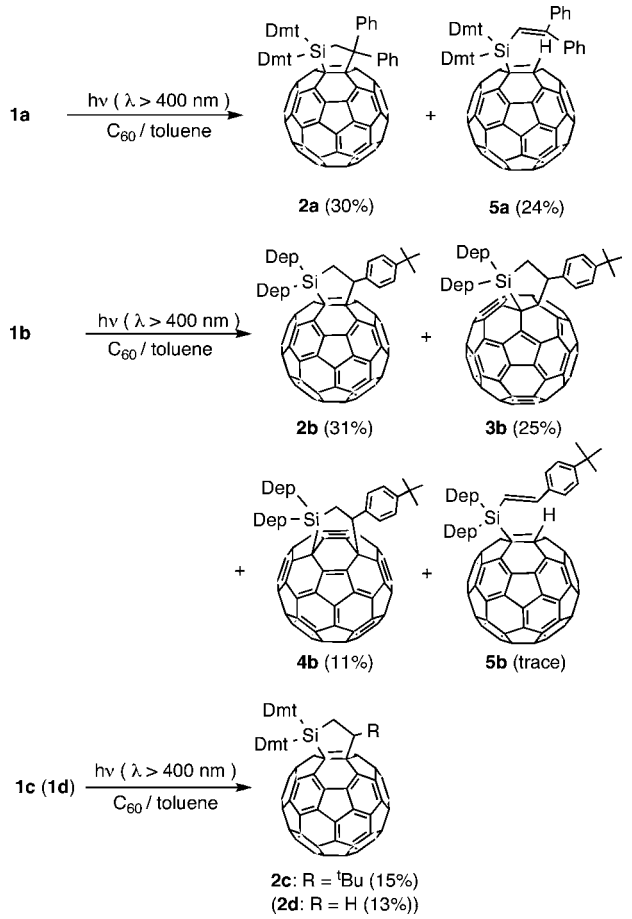

Thermal and photochemical transformation of the silylated products was examined to clarify their relative stabilities. Upon heating toluene solutions of **2b**−**5b** independently at 100 °C in the dark, **3b** afforded **2b**, and **4b** gave a mixture of **2b** and **3b**, respectively, although the conversion of **2b** and **5b** did not take place at all. Meanwhile, irradiation of **2b**−**5b** under the same conditions employed for **1b** at room temperature caused the rearrangement of **4b** to **3b**, although **2b**, **3b**, and **5b** were recovered quantitatively. These results indicate that the stabilities of **2b**, **3b**, and **4b** decrease in the order **2b** > **3b** > **4b** and that the conversion of **4b** to **3b** is likely to occur in part during the photolysis of **1b**. In contrast to **1b**, **1a** produced no product other than **2a** and **5a**. When the photoreaction of C_{60} and **1a** in toluene-d_8 at −30 °C was monitored using ^{1}H NMR, no additional signal suggesting the formation of intermediates was observed.

Structural Determination of 2a and 5a. The MALDI-TOF mass spectrometry of **5a** displays peaks for *m*/*z* 1250 (M^-), 720(C_{60}^-), and 529(M^--$C_{60}H$) as expected for a 1:1 adduct of C_{60} and **1a**, whereas that of **2a** gives no peak for M^-. In the UV−vis absorption spectra of **2a** and **5a**, characteristic absorption maxima are observed, respectively, at 443 nm for **2a**, and at 446 nm for **5a** (Figure 1). Because such absorption bands are known to be specific to C_{60} derivatives resulting from 1,2-addition at a 6,6-ring junction,[18] similar structures of derivatized C_{60} cage are suggested for **2a** and **5a**. Additional structural information was obtained by ^{1}H NMR and ^{13}C NMR spectroscopy as follows.

The ^{1}H NMR spectrum of **2a** displays four methyl, two *tert*-butyl, and four aryl proton signals of the two nonequivalent

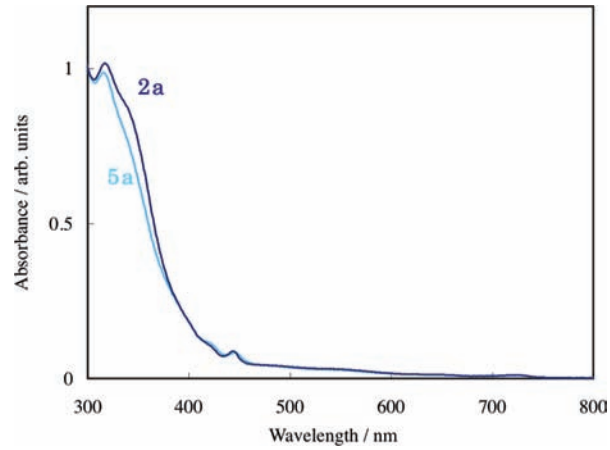

Figure 1. Absorption spectra of **2a** and **5a**.

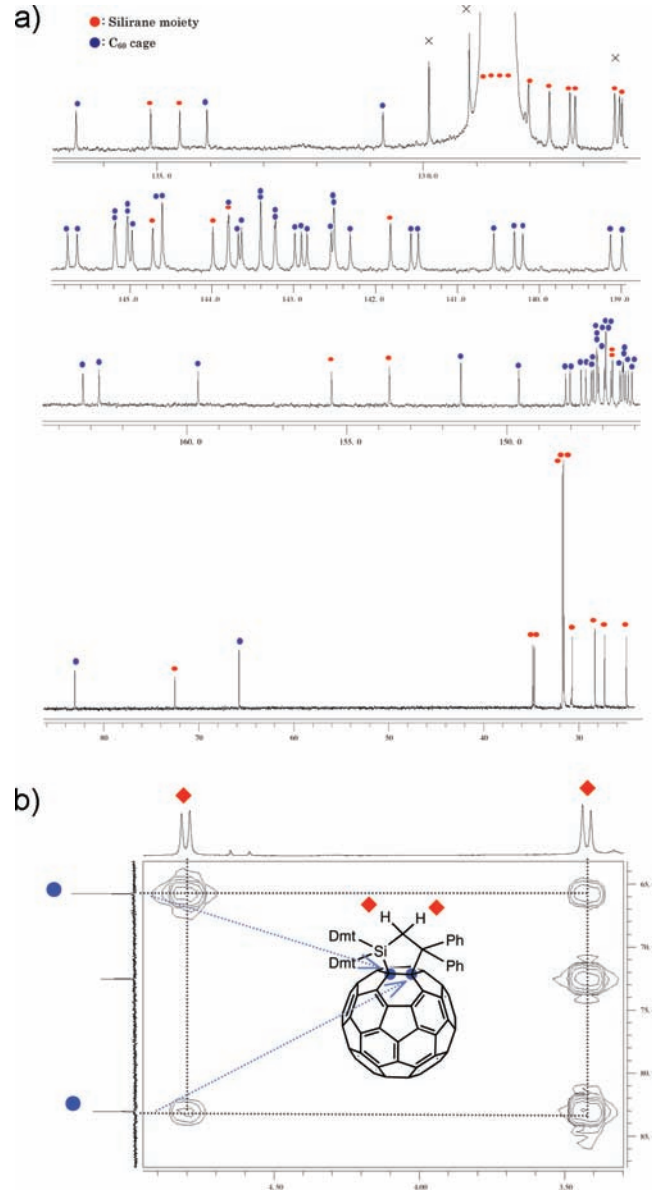

Figure 2. (a) ^{13}C NMR spectrum of **2a**. (b) HMBC spectrum of **2a**.

Dmt groups, as well as those of phenyl protons. Two doublets for the two methylene protons are also observed to suggest an unsymmetrical structure of **2a**. In the ^{13}C NMR spectrum of

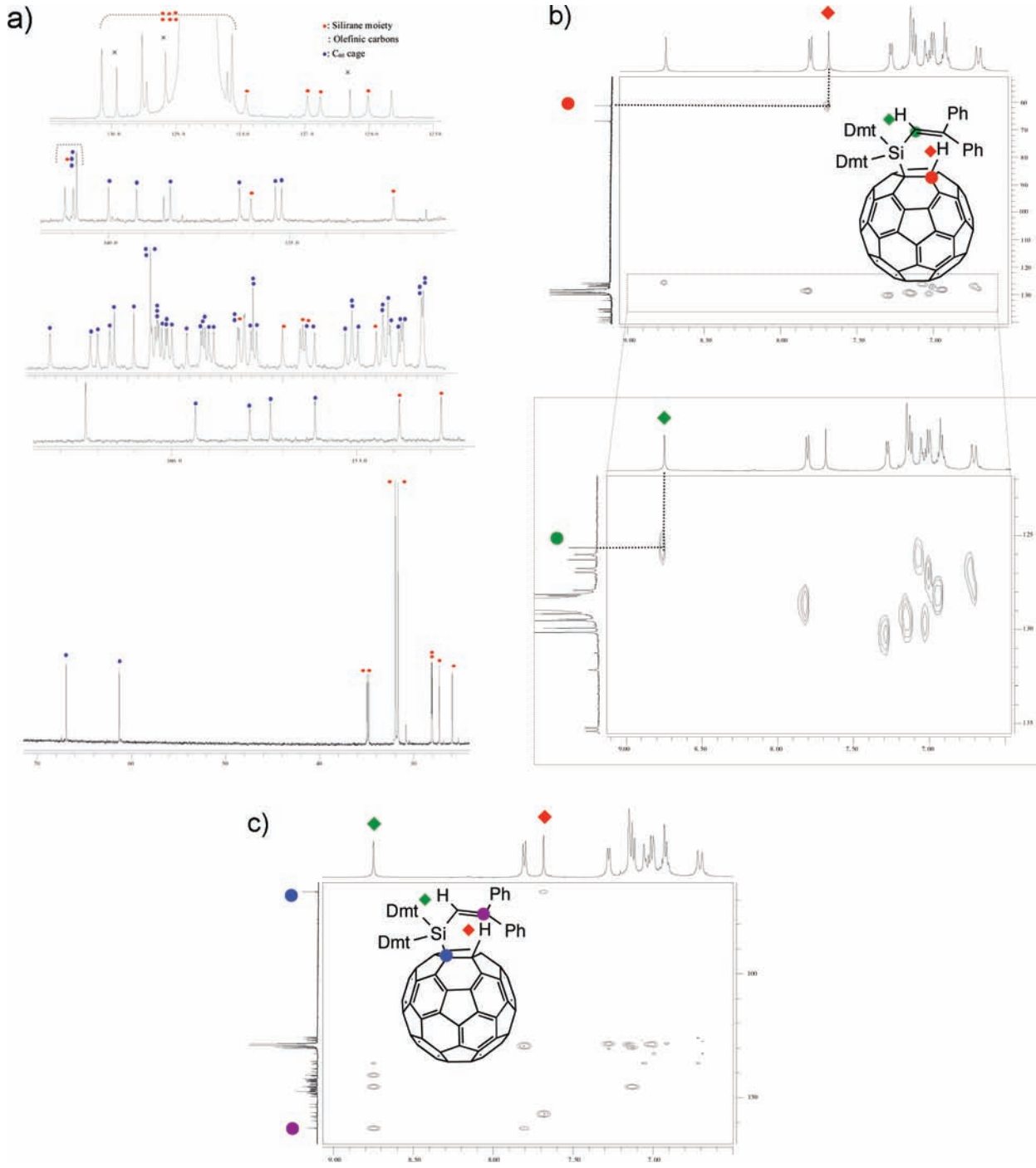

Figure 3. (a) ^{13}C NMR spectrum of **5a**. (b) HMQC spectra of **5a**. (c) HMBC spectrum of **5a**.

2a, 58 signals for the sp^2 carbons of C_{60} skeleton were observed along with 10 tertiary and 12 quaternary sp^2 carbon signals from the two nonequivalent Dmt and the two nonequivalent phenyl groups (Figures 2a). This result also suggests that free rotation of the bulky Dmt rings may be restricted because of the steric hindrance in **2a**. In addition, signals for two sp^3 carbons of the C_{60} cage, one methylene carbon and one quaternary carbon of the silacyclopentane ring of **2a**, and four methyl and two *tert*-butyl carbons of Dmt groups were observed in the upfield spectral area. Moreover, the HMBC spectrum displays cross peaks corresponding to the correlation of the methylene protons and the sp^3 carbons of C_{60} cage and the quaternary carbon of the silacyclopentane ring in **2a** (Figure 2b). These spectral data are consistent with C_1 symmetry of **2a** resulting from 1,2-addition of **1a** at the 6,6-ring junction of C_{60}, with the silacyclopentane ring held in an envelope conformation.

Regarding the ^1H NMR and ^{13}C NMR spectra of **5a**, numbers and multiplicities of the signals for the C_{60} cage, the Dmt, and the phenyl groups closely resemble those of **2a**, except that one of sp^3 carbon (δ 61.31) of the C_{60} cage is tertiary to have a C_{60}−H bond (Figures 3a). In addition, two singlet proton signals are found at δ 8.76 and 7.69, which are assignable, respectively, to the alkenyl proton and the methyne proton on the C_{60} cage of **5a**. The HMQC spectrum of **5a** indicates that these proton signals at δ 8.76 and 7.69 correlate with a signal of the alkenyl carbon at δ 125.66 and that of sp^3 carbon of the C_{60} cage at δ

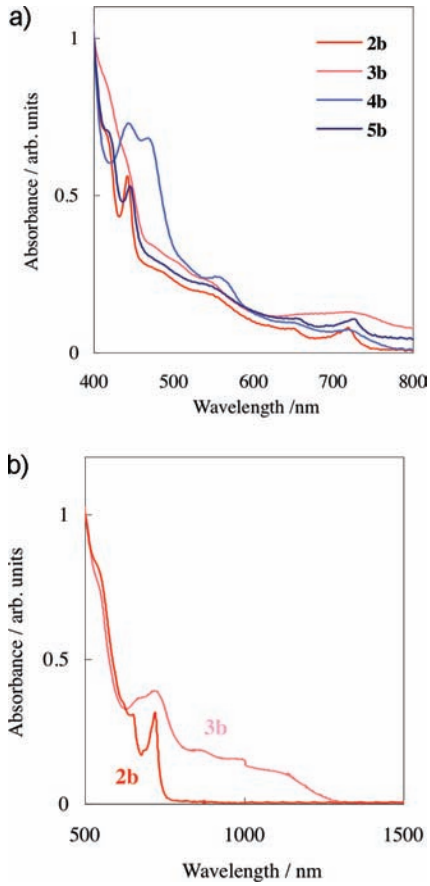

Figure 4. (a) Absorption spectra of **2b**, **3b**, **4b**, and **5b**. (b) vis−NIR spectra of **2b** and **3b**.

61.31, respectively (Figure 3b). Meanwhile, the proton signal at δ 7.69 shows a cross peak with another sp^3 carbon (δ 66.92) of the C_{60} cage in the HMBC spectrum (Figure 3c). These observations support the proposed structure of **5a** as a hydrosilylated C_{60} derivative.

Structural Determination of 2b, 3b, 4b, and 5b. In the MALDI-TOF mass spectrometry, **2b**, **3b**, **4b**, and **5b** each display peaks for *m*/*z* 1174 (M^-), 720(C_{60}^-) as expected for 1:1 adducts of C_{60} and **1b**. The UV−vis absorption spectra of **2b** and **5b** show absorption maxima at 442 nm for **2b** and 444 nm for **5b** (Figure 4a,b). Probably, **2b** and **5b** should be derivatives resulting from 1,2-addition at a 6,6-ring junction of C_{60} as proposed for **2a** and **5a**. In a similar manner, it is suggested that **4b** formed by 1,4-addition to the six-membered ring of C_{60} judged by its characteristic absorption maxima at 443, 467, and 552 nm.[19] On the other hand, no specific absorption band is observed for **3b**, which would yield a clue to the structure, although **3b** has an absorption band extending to a longer wavelength than those of **2b**, **4b**, and **5b**.

The ^{1}H NMR of **2b** displays proton signals for four ethyl groups and one *tert*-butyl group, along with aromatic proton signals of Dep and 4-*tert*-butylphenyl groups. The ring protons of the silacyclopentane addend of **2b** are confirmed to constitute an ABX spin system. Meanwhile, the ^{13}C NMR spectrum of **2b** shows 58 quaternary signals for the C_{60} skeleton together with 16 signals of eight tertiary and eight quaternary aromatic carbons of the two nonequivalent Dep and the 4-*tert*-butylphenyl groups (Figure 5a). As described for **2a**, the degenerated spectral symmetry of Dep groups may be explained based on restriction of the free rotation of bulky Dep rings in **2b**. Also observed are signals corresponding to two sp^3 carbons of the C_{60} cage, one methylene and one methyne of the silacyclopentane ring of **2b**, four ethyl groups, and one *tert*-butyl group. Additional analyses using HMQC and HMBC support the spectral assignment of the silacyclopentane ring protons of **2b** at δ 5.31, 3.94, and 2.55. Consequently, the methylene carbon signal at δ 29.01 show two cross peaks with the proton signals at δ 3.94 and 2.55, whereas the methyne carbon at δ 58.65 correlates with a proton signal at δ 5.31 in the HMQC spectrum (Figure 5b). Moreover, in the HMBC spectrum of **2b**, cross peaks are observed between the sp^3 carbon signals of the C_{60} cage at δ 80.07, 74.84, and the silacyclopentane ring proton signals (Figure 5c). Therefore, it is concluded that **2b** has C_1 symmetry with a silacyclopentane structure at a 6,6-ring junction of C_{60}.

In the ^{1}H NMR and ^{13}C NMR spectra of **3b**, numbers and multiplicities of proton and carbon signals for the C_{60} cage, the Dep, and the 4-*tert*-butylphenyl groups closely resemble those of **2b** (Figure 6a). The presence of a silacyclopentane structure is also suggested by the HMQC and the HMBC spectra (Figures 6b,c). These observations indicate that the structure of **3b** resembles that of **2b** well. However, **3b** was determined to be a closed 1,2-adduct at a 5,6-ring junction of C_{60} using single-crystal X-ray structural analysis as described below.

The NMR analyses of **4b** and **5b** were limited to ^{1}H NMR because of the low yields of these compounds. Although the structure of **4b** was determined to be a 1,4-adduct by single-crystal X-ray analysis, that of **5b** has not been obtained yet. Comparisons of ^{1}H NMR, UV−vis spectra, and MALDI-TOF MS of **5a** and **5b** present the possibility that the structure of **5b** resembles that of **5a**.

Structural Determination of 2c. It can be verified that **2c** and **2d** are the 1:1 adducts because the corresponding molecular ion peaks *m*/*z* 1154 for **2c** and *m*/*z* 1098 for **2d** are observed together with 720 (C_{60}^-) in the MALDI-TOF mass spectra. The characteristic absorption bands for 1,2-adducts at the 6,6-ring junction are also confirmed at 443 nm for **2c** and 442 nm for **2d** in UV−vis spectra. Because **2c** displays four methyl, three *tert*-butyl, and four aryl proton signals in the ^{1}H NMR spectrum, the inhibited free rotation of two nonequivalent Dmt groups is suggested. An ABX coupling is also verified for the silacyclopentane ring protons of **2c** using HMQC spectroscopy. In the ^{13}C NMR spectrum of **2c**, 70 sp^2 carbon signals are assigned to 58 carbons of C_{60} skeleton and four tertiary and eight quaternary aromatic carbons of the two nonequivalent Dmt groups. Additional 14 sp^3 carbon signals are found in the upfield region for the four methyl and the three *tert*-butyl groups and the four silacyclopentane ring carbons of **2c**. Therefore, it is concluded that **2c** is a 1,2-adduct at the 6,6-ring junction as with **2a** and **2b**. The low temperature ^{1}H NMR measurement of **2d** at 223 K provided four methyl, two *tert*-butyl, and four aryl proton signals as well as three signals assignable to the silacyclopentane ring protons. By comparison of the spectral data with those of **2a**-**2c**, **2d** is assumed to be a 1,2-adduct at 6,6-ring junction of C_{60} without free rotation of the Dmt groups and with an envelope conformation of the silacyclopentane ring. Furthermore, coalescence of these signals reflecting conformational change of **2d** was observed at 295 K, yielding an activation energy $\Delta G^{\ddagger} = 15.4$ kcal/mol. The fact that **2d** afforded one methyl, one *tert*-butyl, one aryl proton, and two methylene signals in the

(18) Hirsch, A.; Grösser, T.; Skiebe, A.; Soi, A. *Chem. Ber.* **1993**, *126*, 1061–1067.
(19) Akasaka, T.; et al. *Org. Lett.* **2000**, *2*, 2671–2674.

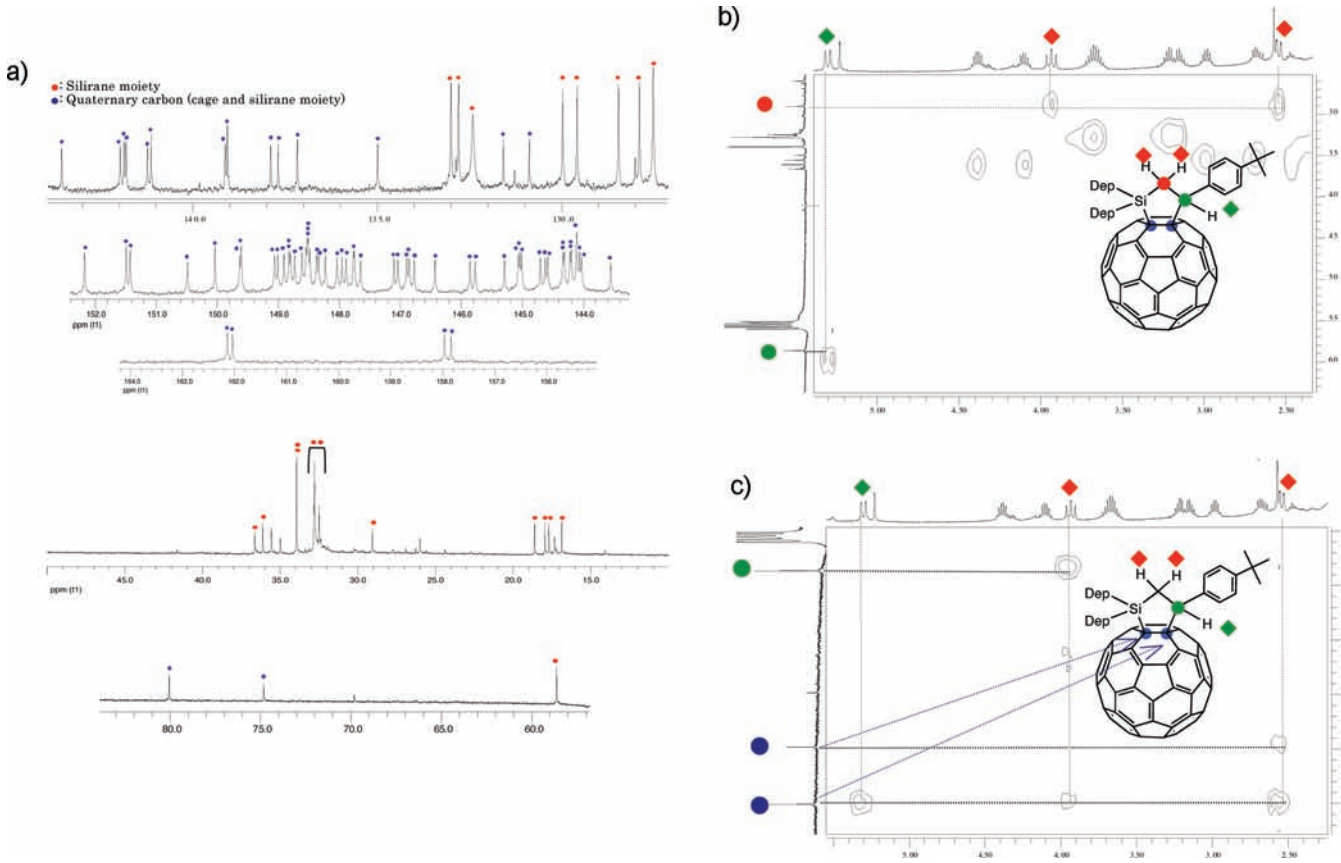

Figure 5. (a) ^{13}C NMR spectrum of **2b**. (b) HMQC spectrum of **2b**. (c) HMBC spectrum of **2b**.

^{1}H NMR measurement at 383 K confirmed the proposed structure of **2d**.

Crystal Structures of 2b, 3b, 4b, and 5a. The structures of **2b**, **3b**, **4b**, and **5a** were confirmed using single-crystal X-ray analyses. The structure of **3b** was established unambiguously to be a closed 1,2-adduct at a 5,6-ring junction of C_{60}. ORTEP drawings of **2b**, **3b**, **4b**, and **5a** are shown in Figures 7a−d and 8a−d, with selected bond lengths in Table 2. Also described are the corresponding calculated bond lengths of the optimized structures obtained by the B3LYP/3-21G** method. On the basis of the structural data, the following features should be pointed out: (i) The Si−C bonds between the C_{60} and the silirane addends in **2b**, **3b**, **4b**, and **5a** are markedly elongated compared with those found in normal Si−C single bonds of organosilanes. This elongation may be attributed to the steric repulsion between the C_{60} cage and the bulky substituents on the Si atoms and also to the β-effect resulting from $\sigma-\pi$ conjugation between the Si−C σ-orbital and the π-orbital of the C_{60} cage. (ii) The C−C bond lengths between two sp^3 carbon atoms of the C_{60} cage of **2b** and **3b** are much longer than those of normal C−C single bonds. (iii) The C−C bond lengths between one sp^3 carbon atom and one sp^2 carbon atom of the C_{60} cage of **2b**, **3b**, **4b**, and **5a** are almost within normal values for C−C single bonds as shown in Table 2. (iv) The geometries of sp^3 carbon atoms of the C_{60} cage of **2b**, **3b**, **4b**, and **5a** are roughly tetrahedral, as verified by the bond angles around those atoms. (v) The double bond characters of C5−C6, C7−C8 of **3b** and C8−C9 of **4b** are apparently enhanced because these bonds are shortened substantially compared to the other C−C bond lengths of the pentagon rings of the C_{60} cages. These results suggest that **3b** and **4b** contain double bonds in the pentagon rings of the C_{60} cage and are in agreement with the fact that **3b** and **4b** are less stable than **2b**, which has no such shortened C−C bonds in the pentagon rings.

Reaction Mechanism. It is apparent that C_{60} is selectively excited in these photoreactions because **1a−d** have no absorption band greater than 400 nm and are inert to irradiation. The photoreactions of C_{60} and **1a−d** were suppressed by addition of 1,4-diazabicyclo[2.2.2]octane (DABCO) or 1,2,4,5-tetramethoxybenzene (TMB), each of which quenches the excited triplet state of C_{60} ($^3C_{60}$*). Meanwhile, the free energy changes (ΔG) of the electron-transfer process from **1a** and **1b** to $^3C_{60}$* in toluene are 7.6 and 13.4 kcal/mol, respectively, according to the Rehm−Weller equation.[20] Previously, we reported that the photoaddition of C_{60} with disilirane **6** proceeds probably through an exciplex resulted from $^3C_{60}$* with **6** in nonpolar solvents.[3] It was also observed that $^3C_{60}$* was quenched efficiently by addition of **6** in the laser flash photolysis.[3d−f] On the basis of these results, a similar reaction mechanism is plausible for **1a−d**, as presented in Scheme 3, where $^3C_{60}$* operates as a key reactive species. Addition of $^3C_{60}$* and silirane produces a diradical intermediate **7**. Subsequent ring closure of **7** affords the cyclized adducts **2a**, **2b**, **3b**, and **4b**, whereas intramolecular hydrogen transfer leads to **5a** and **5b**.

Electronic Properties of 2a, 2b, 3b, 4b, 5a, and 5b. The redox potentials of the silylated products **2a**, **2b**, **3b**, **4b**, **5a**, and **5b** were measured using cyclic voltammetry (CV) and differential pulse voltammetry (DPV) and are listed with those of related compounds in Table 3. The corresponding voltammograms are also presented in Figure 9. The oxidation waves in the CV are

(20) Rehm, D.; Weller, A. *Isr. J. Chem.* **1970**, *8*, 259–271.

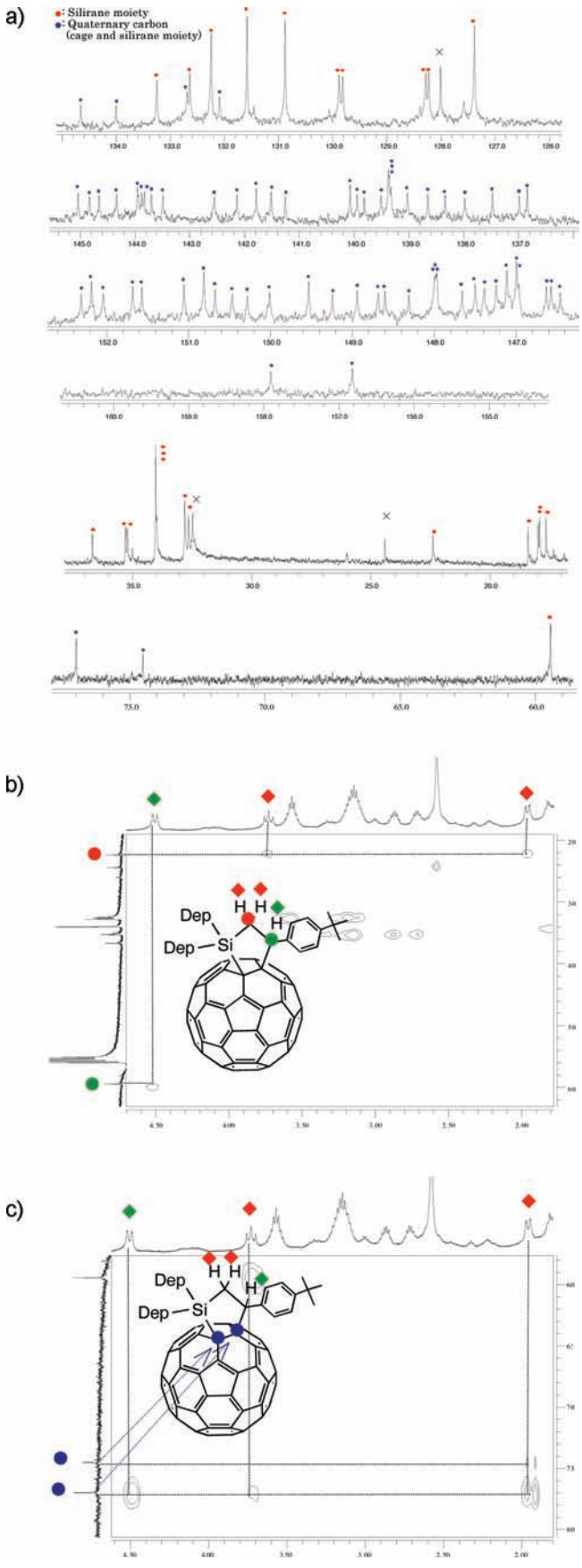

Figure 6. (a) ^{13}C NMR spectrum of **3b**. (b) HMQC spectrum of **3b**. (c) HMBC spectrum of **3b**.

all irreversible, probably because of desilylation during the CV measurements, as observed previously for **8** (Chart 3).[3b] We have reported that the silylated C_{60} show lower oxidation and reduction potentials than those of C_{60} itself and the derivatives with alkyl and alkoxyl substituents.[3b] In fact, the first oxidation potentials (E^{ox}_1) of **2a**, **2b**, **3b**, **4b**, **5a**, and **5b** are shifted cathodically from 130 mV to 530 mV compared to that of C_{60}. Results also show that the E^{ox}_1 values of **2a** and **2b** (1,2-adducts at 6,6-ring junction) and **4b** (1,4-adduct) are somewhat higher than those of the corresponding bis-silylated compounds **8** (1,2-adduct) and **10** (1,4-adduct), respectively. On the other hand, the reduction potentials (E^{red}) of **2a**, **2b**, and **4b** resemble those of **8** and **10** overall. These results indicate that the carbosilylation, compared to the bis-silylation, has medium effects on tuning the electron-donor properties of fullerenes, although their effects on tuning the acceptor properties are similar. Particularly noteworthy is the low E^{ox}_1 and the high E^{red}_1 values of **3b**: the former is comparable with those of **8** and **10**, whereas the latter resembles that of C_{60}. As reported for the **8**, **10**, and **11**, it is also confirmed that the redox properties of the carbosilylated fullerenes depend on both the electronic effects of their substituents and the regiochemistry of the functionality. The 1,2-addition at 5,6-rung junction might exert some specific effects on tuning the redox properties of C_{60}; it is complementary to the 1,2-addition at 6,6-ring junction and the 1,4-addition. Further investigation of the redox properties was conducted based on theoretical calculations as described below.

Theoretical Calculations. To obtain insight into the structures and the electronic properties of the silylated products, theoretical calculations were conducted for **2b**, **3b**, and **4b**. The geometries of the compounds were optimized at the AM1 and the B3LYP/3-21G** levels.[21] Subsequently, single point energies were calculated at the B3LYP/6-31G**//B3LYP/3-21G** level. Figure 10 portrays the optimized structures of **2b**, **3b**, and **4b** with selected bond lengths included in Table 2 for comparison with the corresponding X-ray crystal structures. Checking of these structural parameters confirmed that the calculations reproduce the X-ray structures of the silacyclic vicinities of **2b**, **3b**, and **4b**. The relative energies and the HOMO, LUMO energies of **2b**, **3b**, and **4b** are also listed in Table 4. The relative energies at B3LYP/6-31G**//B3LYP/3-21G** level show that **2b** is 15.5 and 22.8 kcal/mol more stable than **3b** and **4b**, respectively, in agreement with the experimental results of the thermal transformation from **4b** to **2b**. It is particularly interesting that the energy level for HOMO (E_{HOMO}) is raised while that of LUMO (E_{LUMO}) is lowered in **3b** compared to the corresponding levels of **2b** and **4b**, respectively. This result is consistent with the cathodic shifts of E^{ox}_1 and E^{red}_1 of **3b** in comparison with those of **2a**, **2b**, and **4b**.

Conclusions

For this study, C_{60} was derivatized by the photochemical addition of siliranes **1a**−**d** to afford novel carbosilylated compounds, which were characterized using MS, NMR spectroscopy, X-ray crystallography, and electrochemical analyses. Single-crystal X-ray structural analysis of **3b** unambiguously disclosed the structure of a closed 1,2-adduct at 5,6-ring junction of C_{60}, hitherto unknown in the structural determination of fullerene derivatives. Results also show that carbosilylation is

(21) (a) Becke, A. D. *Phys. Rev. A* **1988**, *38*, 3098–3100. (b) Becke, A. D. *J. Chem. Phys.* **1993**, *98*, 5648–5652. (c) Lee, C.; Yang, W.; Parr, R. G. *Phys. Rev. B* **1988**, *37*, 785–789. (d) Frisch, M. J.; et al. *GAUSSIAN 03, rev. C.01*; Gaussian Inc.: Wallingford, CT, 2004.

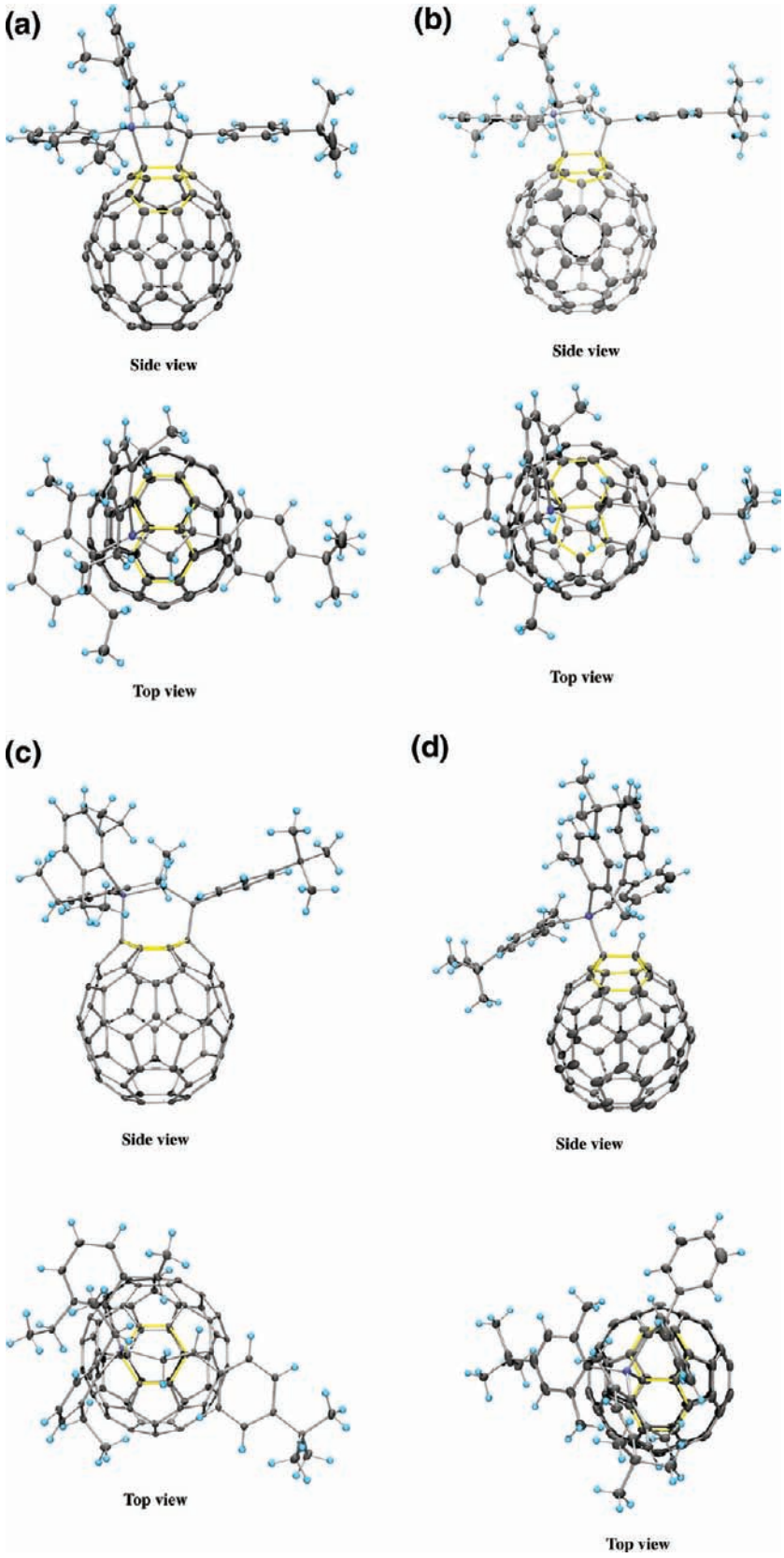

Figure 7. ORTEP drawings of (a) **2b**, (b) **3b**, (c) **4b**, and (d) **5a** with thermal ellipsoids shown at the 30% probability level.

effective for fine-tuning of the redox properties of fullerenes, and complementary to the bis-silylation. Furthermore, it is noteworthy that the redox properties of derivatized fullerenes are controlled not merely by the electronic effect of additives but also by the regiochemistry of addition reactions. These results will broaden the scope of derivatization of fullerenes

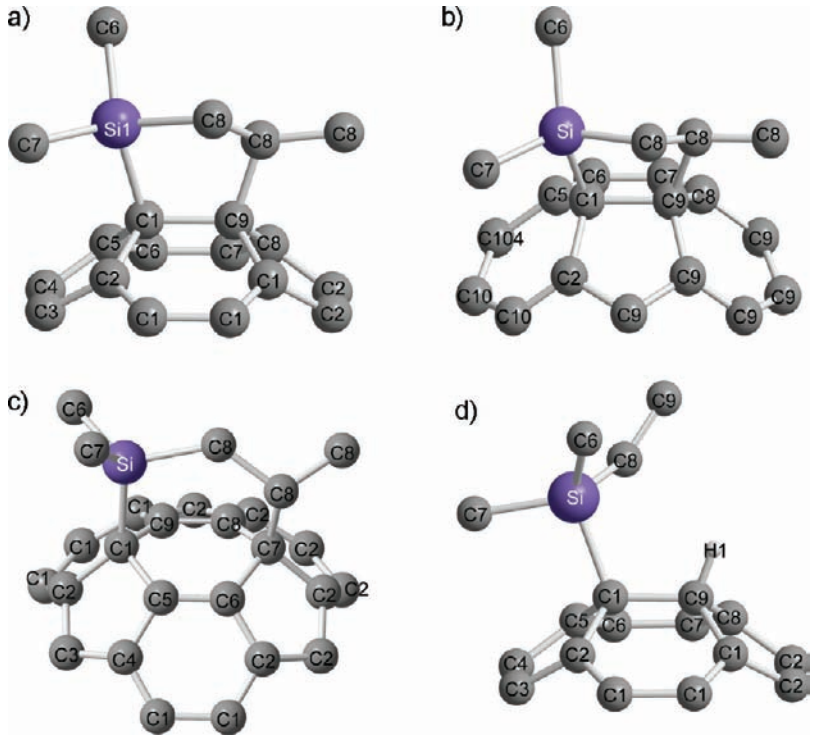

Figure 8. Partial views of (a) **2b**, (b) **3b**, (c) **4b**, and (d) **5a** in the vicinities of addends.

and endohedral metallofullerenes using organosilanes and engender new application of silylated fullerenes for functional materials.

Experimental Section

General. All chemicals and solvents were obtained from Wako Pure Chemical Industries, Ltd. and Aldrich Chemical Co. Inc. and were used without further purification, unless otherwise stated. Toluene was distilled over benzophenone sodium ketyl under an argon atmosphere before its use in reaction. 1,2-D ichlorobenzene (ODCB) was distilled over P_2O_5 under vacuum before its use. High-performance liquid chromatography (HPLC) isolation was performed on LC-908 and LC-918 chromatographs (Japan Analytical Industry Co., Ltd.) that were monitored by UV absorption at 330 nm. Toluene was used as the eluent. Mass spectrometry was performed on a Bruker BIFLEX III instrument (Bruker Analytik) with 1,1,4,4-tetraphenyl-1,3-butadiene as the matrix. Absorption spectra were measured by using a SHIMADZU UV-3150 spectrophotometer (Shimadzu Corp.). The ^{1}H and ^{13}C NMR measurements were conducted on Bruker AVANCE 300 and 500 spectrometers with a CryoProbe system (Bruker Analytik). Cyclic voltammograms (CVs) and differential pulse voltammograms (DPVs) were recorded on a BAS CV50W electrochemical analyzer (BAS Inc.). Platinum wires were used as the working and counter electrodes. The reference electrode was a saturated calomel reference electrode (SCE) filled with 0.1 M $(n\text{-Bu})_4NPF_6$ ($TBAPF_6$) in ODCB. The CVs were recorded using a scan rate of 20 mV/s. The DPVs were obtained using a pulse amplitude of 50 mV, a pulse width of 50 ms, a pulse period of 200 ms, and a scan rate of 20 mV/s.

Photoreactions of C_{60} with Siliranes 1a−d. A typical procedure is exemplified by the case of **1a** as follows. A toluene solution (25 mL) of C_{60} (15.0 mg, 2.1×10^{-5} mol) and **1a** (11.1 mg, 2.1×10^{-5} mol) was degassed using freeze−pump−thaw cycles under reduced pressure. The solution was then irradiated with 500 W tungsten-halogen lamps through a sodium nitrite filter solution (cutoff <400 nm) for 2.5 h. The products **2a** and **5a** were isolated by HPLC using a 5PBB column (i.d. 20 mm × 250 mm) and a Buckey Prep M column (i.d. 20 mm × 250 mm) obtained from Nacalai Tesque inc.

Data for 2a: dark brown solid; ^{1}H NMR (500 MHz, C_6D_6, 293 K) δ 7.15 (s, 1H), 7.11 (s, 1H), 6.78 (s, 1H), 6.74 (s, 1H), 7.16−6.71 (m, 10H), 4.80 (d, 1H, J = 14 Hz), 3.42 (d, 1H, J = 14 Hz), 3.21 (s, 3H), 3.02 (s, 3H), 2.55 (s, 3H), 2.45 (s, 3H), 1.22 (s, 9H), 1.11 (s, 9H); ^{13}C NMR (500 MHz, C_6D_6, 293 K) δ 162.74 (s, 1C), 162.24 (s, 1C), 159.65 (s, 1C), 155.48 (s, 1C), 153.67 (s, 1C), 151.43 (s, 1C), 149.62 (s, 1C), 148.16 (s, 1C), 148.02 (s, 1C), 147.68 (s, 1C), 147.53 (s, 1C), 147.36 (s, 1C), 147.29 (s, 1C), 147.19 (s, 3C), 147.13 (s, 1C), 146.95 (s, 1C), 146.91 (s, 3C), 146.74 (s, 1C), 146.69 (s, 1C), 146.45 (s, 1C), 146.37 (s, 1C), 146.36 (s, 1C), 146.29 (s, 1C), 146.20 (s, 1C), 146.01 (s, 1C), 145.76 (s, 1C), 145.65 (s, 1C), 145.18 (s, 2C), 145.03 (s, 2C), 144.97 (s, 1C), 144.72 (s, 1C), 144.61 (s, 2C), 143.99 (s, 1C), 143.80 (s, 2C), 143.68 (s, 1C), 143.64 (s, 1C), 143.40 (s, 2C), 143.22 (s, 2C), 142.99 (s, 1C), 142.91 (s, 1C), 142.84 (s, 1C), 142.54 (s, 1C), 142.51 (s, 2C), 142.31 (s, 1C), 141.82 (s, 1C), 141.57 (s, 1C), 141.48 (s, 1C), 140.56 (s, 1C), 140.31 (s, 1C), 140.20 (s, 1C), 139.13 (s, 1C), 138.99 (s, 1C), 136.52 (s, 1C), 135.12 (s, 1C), 134.57 (s, 1C), 134.06 (s, 1C), 130.76 (s, 1C), 127.25 (d, 1C), 127.15 (d, 1C), 126.41 (d, 1C), 126.27 (d, 1C), 83.05 (s, 1C; $\underline{C}_{60}C$), 72.53 (s, 1C; $\underline{C}Ph_2$), 65.76 (s, 1C; $\underline{C}_{60}Si$), 34.87 (s, 1C; $\underline{C}(CH_3)_3$), 34.69 (s, 1C; $\underline{C}(CH_3)_3$), 31.70 (4C), 31.58 (q, 3C; $C(\underline{C}H_3)_3$), 30.71 (q, 1C; $\underline{C}H_3$), 28.31 (q, 1C; $\underline{C}H_3$), 27.29 (q, 1C; $\underline{C}H_3$), 24.99 (q, 1C; $\underline{C}H_3$); vis−NIR (toluene) λ_{max} 443, 316 nm; MALDI-TOF MS m/z 720 (C_{60}^-).

Data for 5a: dark brown solid; ^{1}H NMR (500 MHz, C_6D_6) δ 8.76 (s, 1H), 7.80 (d, 2H, J = 8 Hz), 7.69 (s, 1H), 7.28 (d, 2H, J = 7 Hz), 7.16−6.93 (m, 6H), 7.07 (s, 1H), 7.01 (s, 1H), 6.73 (s, 1H), 6.70 (s, 1H), 3.45 (s, 3H), 3.01 (s, 3H), 2.36 (s, 3H), 2.06 (s, 3H), 1.36 (s, 9H), 1.04(s, 9H); ^{13}C NMR (500 MHz, C_6D_6) δ 162.33 (d, 1C; $\underline{C}H$), 159.37 (s, 1C), 157.89 (s, 1C), 157.33 (s, 1C), 156.13 (s, 1C), 153.85 (s, 1C), 152.72 (s, 1C), 149.50 (s, 1C), 148.72 (s, 1C), 148.58 (s, 1C), 148.35 (s, 1C), 148.26 (s, 1C), 147.88 (s, 1C), 147.56 (s, 3C), 147.53 (s, 1C), 147.45 (s, 1C), 147.43 (s, 1C), 147.39 (s, 1C), 147.34 (s, 1C), 147.26 (s, 1C), 147.23 (s, 1C),

Table 2. Selected Bond Lengths (Å) of **2b**, **3b**, **4b**, and **5a**

bond	length[a]
2b	
Si1−C1	2.005(2) [2.019]
Si1−C81	1.882(3) [1.900]
C1−C9	1.611(3) [1.619]
C9−C82	1.583(3) [1.586]
C81−C82	1.537(2) [1.560]
C1−C2	1.532(2) [1.542]
C1−C5	1.521(3) [1.529]
C9−C10	1.526(3) [1.541]
C9−C8	1.544(2) [1.540]
3b	
Si1−C1	1.999(2) [2.013]
Si1−C81	1.893(2) [1.900]
Si1−C61	1.926(2) [1.924]
Si1−C71	1.903(2) [1.898]
C1−C9	1.637(3) [1.660]
C9−C82	1.585(3) [1.583]
C81−C82	1.542(3) [1.560]
C1−C2	1.535(3) [1.545]
C1−C5	1.506(3) [1.500]
C9−C94	1.634(2) [1.539]
C8−C9	1.524(3) [1.511]
C5−C6	1.368(3) [1.387]
C7−C8	1.384(3) [1.384]
4b	
Si1−C1	1.991(2) [1.998]
Si1−C81	1.936(2) [1.971]
Si1−C61	1.901(2) [1.917]
Si1−C71	1.902(2) [1.922]
C1−C5	1.526(2) [1.525]
C5−C6	1.357(2) [1.359]
C6−C7	1.516(2) [1.534]
C7−C8	1.505(2) [1.500]
C8−C9	1.359(2) [1.358]
C1−C9	1.496(2) [1.509]
C81−C82	1.569(2) [1.608]
C7−C82	1.573(2) [1.581]
5a	
Si1−C1	1.991(2)
Si1−C85	1.876(3)
C1−C9	1.590(3)
C1−C2	1.529(3)
C1−C5	1.533(3)
C9−C10	1.524(4)
C9−C8	1.538(3)

[a] Bond lengths of optimized structures at the B3LYP/3-21G** level are in brackets.

Scheme 3

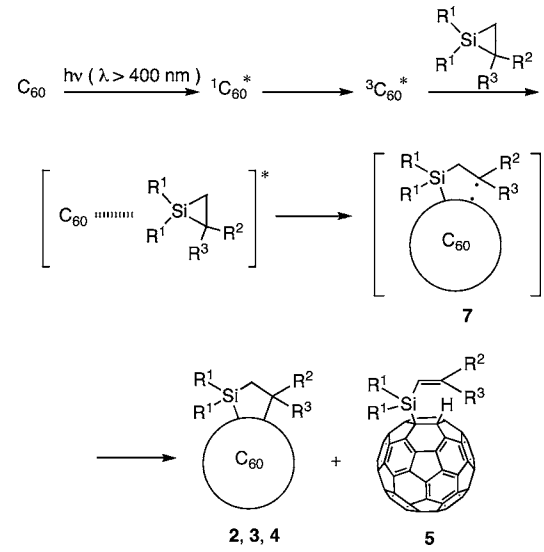

Table 3. Redox Potentials (V)[a] of Silylated C_{60} Derivatives

compound	E^{ox}_1	E^{red}_1	E^{red}_2	E^{red}_3
2a	+0.99[b,c]	−1.28[d]	−1.66[d]	−2.23[d]
5a	+0.90[b,c]	−1.31[c]	−1.72[c]	−2.19[c]
2b	+1.08[b,d]	−1.28[d]	−1.74[d]	−2.28[d]
3b	+0.68[b,e]	−1.15[e]	−1.73[e]	
4b	+0.82[b,c]	−1.25[c]	−1.68[c]	
5b	+0.94[b,c]	−1.24[c]	−1.68[c]	−2.24[c]
C_{60}[f]	+1.21[b]	−1.12	−1.50	−1.95
8[f]	+0.60[b]	−1.29	−1.67	−2.18
9[g]	+0.77[b]	−1.21	−1.57	−1.97
10[h]	+0.73[b]	−1.22	−1.61	−2.12
11[h]	+0.33[b]	−1.19	−1.59	−2.18

[a] Values obtained by DPV are in volts relative to ferrocene/ferrocenium couple. [b] Irreversible. [c] 50 mV/s scan rate. [d] 20 mV/s scan rate. [e] 100 mV/s scan rate. [f] Reference 3b. [g] Reference 4d. [h] Reference 4a.

147.14 (s, 1C), 146.86 (s, 1C), 146.58 (s, 1C), 146.55 (s, 1C), 146.50 (s, 1C), 146.43 (s, 1C), 146.33 (s, 1C), 145.87 (s, 1C), 145.84 (s, 1C), 145.75 (s, 1C), 145.61 (s, 1C), 145.57 (s, 2C), 145.50 (s, 1C), 145.00 (s, 1C), 144.66 (s, 1C), 144.61 (s, 1C), 144.56 (s, 1C), 144.38 (s, 1C), 143.79 (s, 1C), 143.66 (s, 2C), 146.54 (s, 1C), 143.18 (s, 1C), 143.05 (s, 2C), 142.96 (s, 1C), 142.92 (s, 1C), 142.75 (s, 1C), 142.71 (s, 1C), 142.67 (s, 1C), 142.31 (s, 2C), 142.28 (s, 2C), 141.20 (s, 1C), 140.97 (s, 1C), 140.88 (s, 2C), 140.00 (s, 1C), 139.23 (s, 1C), 138.30 (s, 1C), 136.39 (s, 1C), 136.08 (s, 1C), 135.41 (s, 1C), 135.23 (s, 1C), 132.14 (s, 1C), 130.16 (d, 1C), 129.53 (d, 1C), 129.46 (d, 1C), 128.84 (d, 1C), 128.20 (d, 1C), 128.13 (d, 1C), 127.91(d, 1C), 126.96 (d, 1C), 126.76 (d, 1C), 126.02 (d, 1C), 125.66 (s, 1C; $\underline{C}Ph_2$), 66.92 (s, 1C; $\underline{C}_{60}Si$), 61.31 (d, 1C; $\underline{C}_{60}H$), 34.96(s, 1C; $\underline{C}(CH_3)_3$), 34.80 (s, 1C; $\underline{C}(CH_3)_3$), 31.97 (q, 3C; $C(\underline{C}H_3)_3$), 31.68 (q, 3C; $C(\underline{C}H_3)_3$), 28.11 (q, 1C; $\underline{C}H_3$), 28.05 (q, 1C; $\underline{C}H_3$), 27.30 (q, 1C; $\underline{C}H_3$), 25.92 (q, 1C; $\underline{C}H_3$); vis−NIR (toluene) λ_{max} 446, 316 nm; MALDI-TOF MS *m/z* 1250 (M^-), 720 (C_{60}^-), 529 (M^--$C_{60}H$).

Data for 2b: dark brown solid; ^{1}H NMR (500 MHz, CS_2/CD_2Cl_2, 293 K) δ 7.66−7.02 (m, 10H), 5.31(dd, 1H, J = 15 Hz, J = 2 Hz), 4.42−4.35 (m, 1H), 4.14−4.06 (m, 1H), 3.94 (dd, 1H, J = 15 Hz, J = 13 Hz), 3.74−3.60 (m, 2H), 3.26−3.11 (m, 2H), 3.02−2.95 (m, 1H), 2.72−2.63 (m, 1H), 2.55 (dd, 1H, J = 13 Hz, J = 2 Hz), 1.94 (t, 3H, J = 7 Hz), 1.78 (t, 3H, J = 7 Hz), 1.49 (s, 9H), 0.92 (t, 3H, J = 7 Hz), 0.57 (t, 3H, J = 7 Hz); ^{13}C NMR (500 MHz, CS_2/CD_2Cl_2, 293 K) δ 162.14 (s, 1C), 162.04 (s, 1C), 159.97 (s, 1C), 157.84 (s, 1C), 152.18 (s, 1C), 151.50 (s, 1C), 151.43 (s, 1C), 150.49 (s, 1C), 150.04 (s, 1C), 149.64 (s, 1C), 149.61 (s, 1C), 149.07 (s, 1C), 149.01 (s, 1C), 148.92 (s, 1C), 148.93 (s, 1C), 148.81 (s, 1C), 148.74 (s, 1C), 148.62 (s, 1C), 148.55 (s, 1C), 148.53 (s, 1C), 148.49 (s, 1C), 148.38 (s, 1C), 148.35 (s, 1C), 148.24 (s, 1C), 148.04 (s, 1C), 147.96 (s, 1C), 147.90 (s, 1C), 147.78 (s, 1C), 147.11 (s, 1C), 147.05 (s, 1C), 146.90 (s, 1C), 146.78 (s, 1C), 146.44 (s, 1C), 146.87 (s, 1C), 145.78 (s, 1C), 145.30 (s, 1C), 145.07 (s, 1C), 145.05 (s, 1C), 145.02 (s, 1C), 144.71 (s, 1C), 144.64 (s, 1C), 144.60 (s, 1C), 144.35 (s, 1C), 144.32 (s, 1C), 144.23 (s, 1C), 144.21 (s, 1C), 144.12 (s, 1C), 144.01 (s, 1C), 144.04 (s, 1C), 143.56 (s, 1C), 141.97 (s, 1C), 141.87 (s, 1C), 141.81 (s, 1C), 141.23 (s, 1C), 141.13 (s, 1C), 139.12 (s, 1C), 139.07 (s, 1C), 137.89 (s, 1C), 137.69 (s, 1C), 137.17 (s, 1C), 134.99 (s, 1C), 133.00 (d, 1C), 132.78 (d, 1C), 132.41 (d, 1C), 134.58 (s, 1C), 130.88 (s, 1C), 129.98 (d, 1C), 129.58 (d, 1C), 128.46 (d, 1C), 127.89 (d, 1C), 127.52 (d, 1C), 80.07 (s, 1C; $\underline{C}_{60}C$), 74.84 (s, 1C; $\underline{C}_{60}Si$), 58.65 (d, 1C; $C_{60}\underline{C}H$), 36.66 (t, 1C; $\underline{C}H_2$), 36.14 (t, 1C; $\underline{C}H_2$), 33.97 (t, 2C; $\underline{C}H_2$), 32.85 (s, 4C), 32.82 (t, 1C; $\underline{C}H_2$), 29.01 (q, 1C; $\underline{C}H_3$), 18.64 (q, 1C; $\underline{C}H_3$), 17.98 (q, 1C; $\underline{C}H_3$), 17.72 (q, 1C; $\underline{C}H_3$), 16.89 (q, 1C; $\underline{C}H_3$);

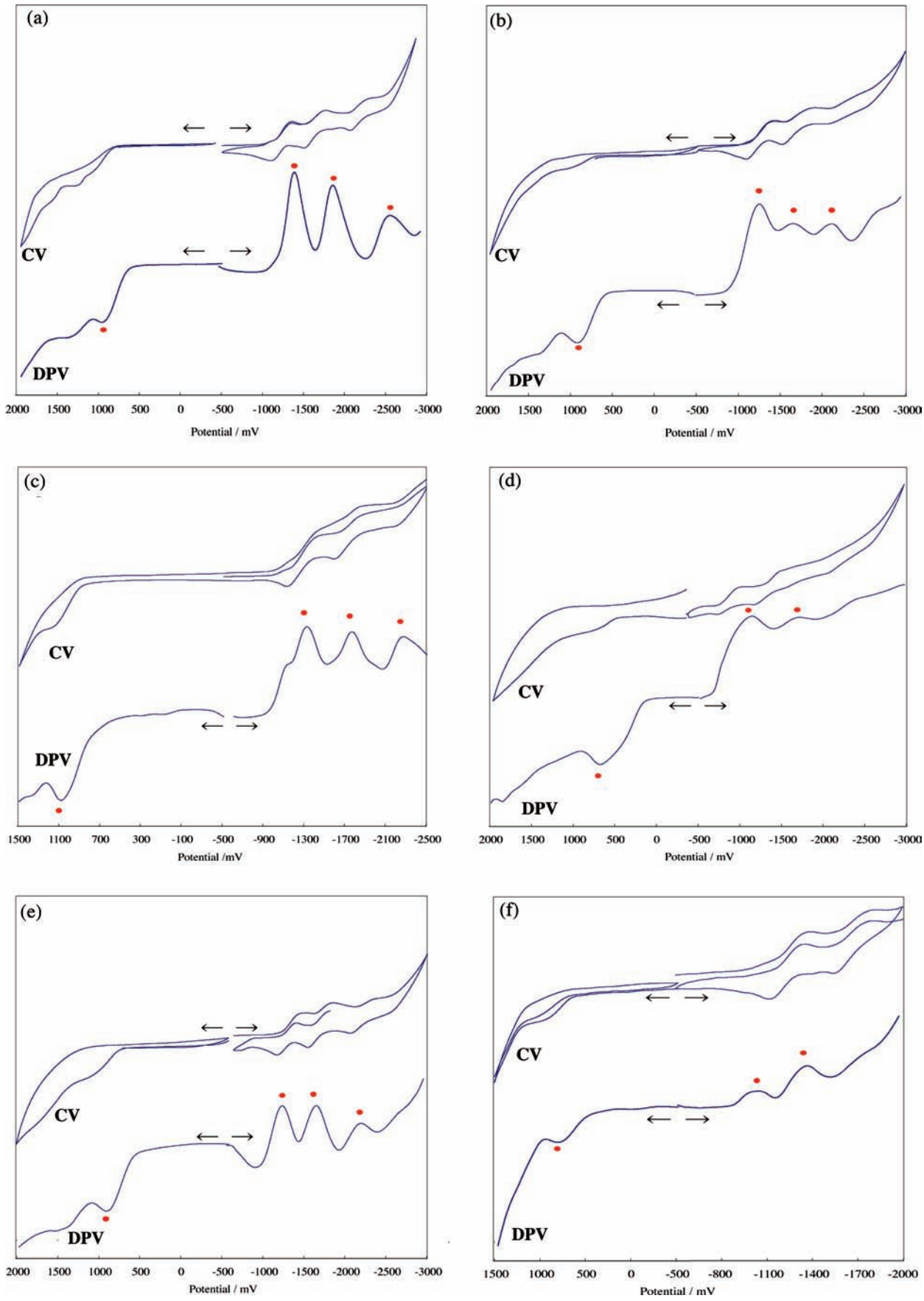

Figure 9. Cyclic voltammograms (CV) and differential pulse voltammograms (DPV) of **2a** (a), **5a** (b), **2b** (c), **3b** (d), **4b** (e), and **5b** (f) in 1,2-dichlorobenzene containing 0.1 M (*n*-butyl)$_4$NPF$_6$. The peaks of monosilylated C_{60} derivatives are marked by red ●. Condition: working electrode, Pt disk (1 mm diameter); counter electrode, Pt wire; reference electrode, SCE. Redox potentials are in volts relative to ferrocene/ferrocenium couple.

Chart 3

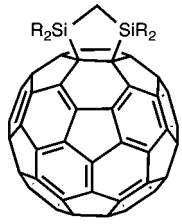

8 (R = Mes)

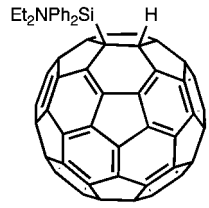

9

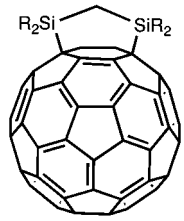

10 (R = Dep)

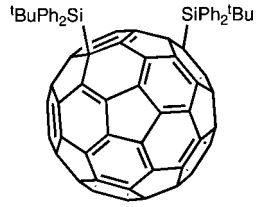

11

vis−NIR (toluene) λ_{max} 719, 442 nm; MALDI-TOF MS *m*/*z* 1274 (M^-), 720 (C_{60}^-).

Data for 3b: dark brown solid; ^{1}H NMR (500 MHz, CS_2/CD_2Cl_2, 293 K) δ 7.71−7.12 (m, 10H), 4.51 (dd, 1H, J = 15 Hz, J = 2 Hz), 3.74 (dd, 1H, J = 15 Hz, J = 13 Hz), 3.62−3.51 (m, 2H), 3.21−3.08 (m, 4H), 2.89−2.69 (m, 2H), 1.97 (dd, 1H, J = 13 Hz, J = 2 Hz), 1.68 (t, 3H, J = 7 Hz), 1.64 (t, 3H, J = 7 Hz), 1.50 (s, 9H), 0.93 (t, 3H, J = 7 Hz), 0.53 (t, 3H, J = 7 Hz); ^{13}C NMR (500 MHz, CS_2/CD_2Cl_2, 293 K) δ 157.91 (s, 1C), 156.82 (s, 1C), 152.31 (s, 1C), 152.19 (s, 1C), 152.04 (s, 1C), 151.68 (s, 1C), 151.57 (s, 1C), 151.06 (s, 1C), 150.81 (s, 1C), 150.68 (s, 1C), 150.47 (s, 1C), 150.28 (s, 1C), 150.01 (s, 1C), 149.53 (s, 1C), 149.24 (s, 1C), 148.94 (s, 1C), 148.68 (s, 1C), 148.60 (s, 1C), 148.31 (s, 1C), 148.00 (s, 1C), 147.98 (s, 1C), 147.97 (s, 1C), 147.66 (s, 1C), 147.50 (s, 1C), 147.39 (s, 1C), 147.24 (s, 1C), 147.21 (s, 1C), 146.99 (s, 2C), 146.63 (s, 1C), 146.57 (s, 1C), 146.46 (s, 1C), 145.04 (s, 1C), 144.83 (s, 1C), 144.66 (s, 1C), 144.33 (s, 1C), 143.95 (s, 1C), 143.88 (s, 1C), 143.83 (s, 1C), 143.70 (s, 1C), 143.49 (s, 1C), 142.55 (s, 1C), 142.14 (s, 1C), 141.79 (s, 1C), 141.51 (s, 1C), 141.26 (s, 1C), 140.07 (s, 1C), 139.95 (s, 1C), 139.82 (s, 1C), 139.51 (s, 1C), 139.38 (s, 2C), 139.33 (s, 1C), 139.03 (s, 1C), 138.66 (s, 1C), 138.34 (s, 1C), 137.99 (s, 1C), 137.48 (s, 1C), 136.99 (s, 1C), 136.84 (s, 1C), 134.66 (s, 1C), 134.00 (s, 1C), 133.25 (d, 1C), 132.69 (s, 1C), 132.64 (d, 1C), 132.25 (d, 1C), 132.10 (s, 1C), 131.68 (d, 1C), 130.88 (d, 1C), 129.89 (d, 1C), 129.82 (d, 1C), 128.28 (d, 1C), 128.23 (d, 1C), 127.38 (d, 1C), 76.98 (s, 1C; $\underline{C_{60}}C$), 74.52 (s, 1C; $\underline{C_{60}}Si$), 59.43 (d, 1C; $C_{60}\underline{C}H$), 36.69 (s, 1C; $\underline{C}(CH_3)_3$), 35.30 (t, 1C; $\underline{C}H_2$), 35.22 (t, 1C; $\underline{C}H_2$), 34.03 (q, 3C; $C(\underline{C}H_3)_3$), 32.65 (t, 1C; $\underline{C}H_2$), 32.48 (t, 1C; $\underline{C}H_2$), 22.40 (t, 1C; $\underline{C}H_2$), 18.41 (q, 1C; $\underline{C}H_3$), 17.98 (q, 1C; $\underline{C}H_3$), 17.92 (q, 1C; $\underline{C}H_3$), 17.66 (q, 1C; $\underline{C}H_3$); vis−NIR (toluene) no absorption maximum; MALDI-TOF MS *m*/*z* 1274 (M^-), 720 (C_{60}^-).

Data for 4b: dark brown solid; ^{1}H NMR (300 MHz, CS_2/CD_2Cl_2, 293 K) δ 7.97−7.11 (m, 10H), 5.01 (dd, 1H, J = 10 Hz, J = 5 Hz), 4.16 (dd, 1H, J = 15 Hz, J = 10 Hz), 3.53−3.22 (m, 4H), 3.01−2.82 (m, 4H), 2.64 (dd, 1H, J = 15 Hz, J = 5 Hz), 1.84 (t, 3H, J = 7 Hz), 1.68 (t, 3H, J = 7 Hz), 1.60 (s, 9H), 0.78 (t, 3H, J = 7 Hz), 0.64 (t, 3H, J = 7 Hz); vis−NIR (toluene) λ_{max} 552, 467, 443 nm; MALDI-TOF MS *m*/*z* 1274 (M^-), 720 (C_{60}^-).

Data for 5b: dark brown solid; vis−NIR (toluene) λ_{max} 726, 445 nm; MALDI-TOF MS *m*/*z* 1274 (M^-), 720 (C_{60}^-).

Data for 2c: dark brown solid; ^{1}H NMR (300 MHz, C_6D_6/CS_2, 293 K) δ 7.36(s, 1H), 7.12(s, 1H), 7.09(s, 1H), 6.80(s, 1H), 3.67(m, 1H), 3.23(s, 3H), 2.95(m 1H), 2.62(s, 3H), 2.34(s, 3H), 2.07(s, 3H), 1.98(m, 1H), 1.00(s, 9H), 0.98(s, 9H), 0.81(s, 9H); ^{13}C NMR (125 MHz, C_6D_6, 293 K) δ 161.5(s, 1C), 160.1 (s, 1C), 157.5 (s, 1C), 156.9 (s, 1C), 153.6 (s, 1C), 152.7 (s, 1C), 149.4 (s, 1C), 147.4 (s, 1C), 146.8 (s, 1C), 146.7 (s, 3C), 146.6 (s, 1C), 146.5 (s, 1C), 146.4 (s, 2C), 146.3 (s, 3C), 145.8 (s, 1C), 145.7 (s, 1C), 145.6 (s, 3C), 145.5 (s, 2C), 145.0 (s, 2C), 144.5 (s, 2C), 144.4 (s, 1C), 144.0 (s, 1C), 143.8 (s, 1C), 143.7 (s, 1C), 143.3 (s, 1C), 143.2 (s, 3C), 143.1 (s, 1C), 143.0 (s, 1C), 142.8 (s, 1C), 142.6 (s, 1C), 142.5 (s, 1C), 142.4 (s, 1C), 142.2 (s, 1C), 142.1 (s, 1C), 142.0 (s, 1C), 141.8 (s, 1C), 140.2 (s, 1C), 139.6 (s, 1C), 139.2 (s, 1C), 138.5 (s, 1C), 137.2 (s, 1C), 136.2 (s, 1C), 136.0 (s, 1C), 132.8 (s, 1C), 132.6 (s, 1C), 124.8 (s, 1C), 125.2 (s, 1C), 124.6 (s, 1C), 124.3 (s, 1C), 75.6 (s, 1C), 74.6 (s, 1C), 62.9(d, 1C; $SiCH_2\underline{C}H$), 35.5 (s, 1C; tBu), 33.0 (s, 2C; tBu), 29.9 (q, 3C; tBu), 29.8 (q, 3C; tBu), 29.7 (q, 3C; tBu), 28.0 (q, 1C; $\underline{C}H_3$), 25.1 (q, 1C; $\underline{C}H_3$), 24.1 (q, 1C; $\underline{C}H_3$), 22.7 (q, 1C; $\underline{C}H_3$), 20.5 (t, 1C; $Si\underline{C}H_2$); vis−NIR (toluene) λ_{max} 312, 443 nm; MALDI-TOF MS *m*/*z* 1154 (M^-), 720 (C_{60}^-).

Data for 2d: dark brown solid; ^{1}H NMR (300 MHz, C_6D_6/CS_2, 383 K) δ 6.83(s, 4H), 3.48(t, 2H, J = 6.6 Hz), 2.56(s, 12H), 2.31(t, 2H, J = 6.6 Hz), 1.02(s, 18H); ^{1}H NMR (300 MHz, C_6D_6/CS_2, 223 K) δ 7.15(s, 1H), 6.98(s, 1H), 6.90(s, 1H), 6.71(s, 1H), 3.72(m, 2H), 3.35(s, 3H), 3.00(m, 1H), 2.84(s, 3H), 2.37(s, 3H), 2.21(s, 3H), 2.02(m, 1H), 1.34(s, 9H), 1.16(s, 9H); vis−NIR (toluene) λ_{max} 310, 330, 443 nm; MALDI-TOF MS *m*/*z* 1098 (M^-), 720 (C_{60}^-).

X-ray Crystallography of 2b, 3b, 4b, and 5a. Crystals of **2b** were obtained using liquid−liquid bilayer diffusion method of an ODCB solution of **2b** using hexane as a poor solvent. Crystals of **4b** and **5a** were obtained by slow evaporation of the corresponding solutions in mixed solvents of CS_2 and toluene. Mixed crystals of **2b** and **3b** were also obtained using a similar procedure from a solution containing **2b** and **3b** in a mixed solvent of CS_2 and toluene. Single-crystal X-ray diffraction data of **2b** were collected on a Rigaku Saturn CCD area detector (Rigaku Corp.) with graphite monochromated Mo−Kα radiation. Those of **4b**, **5a**, and mixed crystals of **2b** and **3b** were collected on a Rigaku RAXIS-RAPID IP area detector (Rigaku Corp.).

Crystal Data for 2b: $C_{92}H_{42}Si$, M_r = 1175.43, black platelet, 0.20 × 0.13 × 0.11 mm^3, monoclinic, $P2_1/n$ (No. 14), a = 12.777(3), b = 23.903(5), c = 18.151(4) Å, β = 106.495(4)°, V = 5315(2) Å^3, Z = 4; ρ_{calcd} = 1.469 g cm^{-3}, μ(Mo Kα) = 0.105 mm^{-1}, θ_{max} = 29.57°, T = 100.1 K, 38,924 measured reflections, 14,592 independent reflections, 839 refined parameters, GOF = 1.024, R_1 = 0.1346 and wR_2 = 0.2675 for all data; R_1 = 0.0869 for 8633 independent reflections ($I > 2.0\sigma(I)$), largest difference peak and hole 1.45 and −0.50 e Å^{-3}, respectively.

Crystal Data for 2b and 3b: (**2b** and **3b** made mixed crystals in a mixing ratio of 61 (**2b**):39 (**3b**), respectively) $C_{92}H_{42}Si$, M_r = 1175.43, black block, 0.10 × 0.10 × 0.10 mm^3, monoclinic, $P2_1/n$ (No. 14), a = 12.7665(5), b = 23.9369(10), c = 18.2436(6) Å, β = 106.8259(10)°, V = 5336.4(4) Å^3, Z = 4; ρ_{calcd} = 1.463 g cm^{-3}, μ(Mo Kα) = 0.104 mm^{-1}, θ_{max} = 27.39°, T = 120.1 K, 40,593 measured reflections, 11,992 independent reflections, 1291 refined parameters, GOF = 1.028, R_1 = 0.0926 and wR_2 = 0.1784 for all data; R_1 = 0.0630 for 8482 independent reflections ($I > 2.0\sigma(I)$), largest difference peak and hole 0.59 and −0.34 e Å^{-3}, respectively.

Crystal Data for 4b·(C_7H_8)$_2$: $C_{106}H_{58}Si$, M_r = 1359.71, black block, 0.74 × 0.40 × 0.40 mm^3, monoclinic, $P2_1/n$ (No. 14), a = 19.694(4), b = 13.366(2), c = 24.195(4) Å, β = 90.091(8)°, V = 6369.0(18) Å^3, Z = 4; ρ_{calcd} = 1.418 g cm^{-3}, μ(Mo Kα) = 0.098 mm^{-1}, θ_{max} = 27.49°, T = 100.1 K, 61,116 measured reflections, 14,522 independent reflections, 965 refined parameters, GOF = 1.030, R_1 = 0.0734 and wR_2 = 0.1833 for all data; R_1 = 0.0665 for 12,708 independent reflections ($I > 2.0\sigma(I)$), largest difference peak and hole 2.14 and −0.83 e Å^{-3}, respectively.

Crystal Data for 5a·(C_7H_8): $C_{105}H_{54}Si$, M_r = 1343.67, black prism, 0.58 × 0.34 × 0.20 mm^3, monoclinic, $P2_1/c$ (No. 14), a = 14.287(2), b = 23.441(5), c = 19.533(3) Å, β = 104.270(5)°, V = 6339.8(18) Å^3, Z = 4; ρ_{calcd} = 1.408 g cm^{-3}, μ(Mo Kα) =

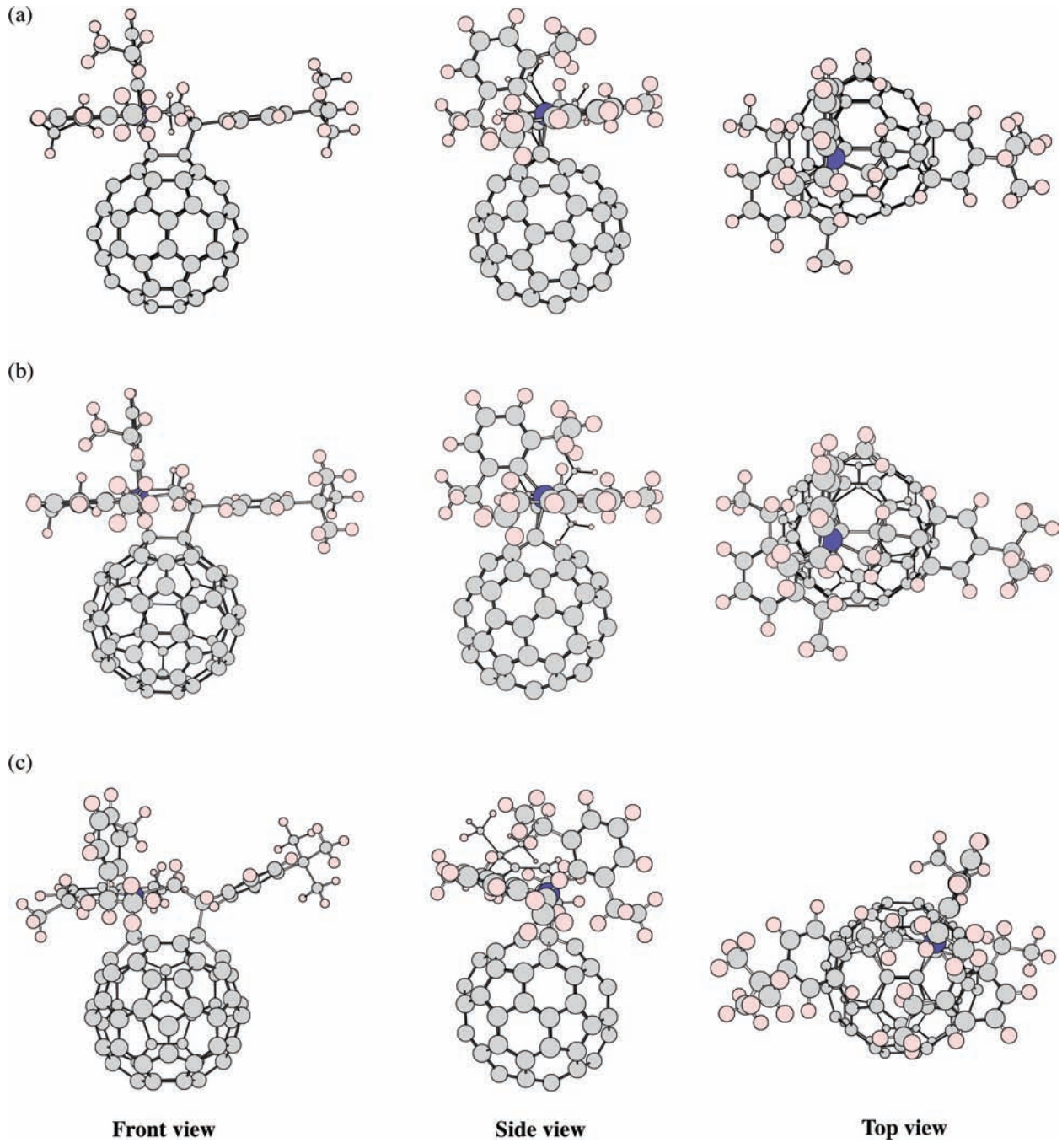

Figure 10. Optimized structures of **2b** (a), **3b** (b), and **4b** (c) at the B3LYP/3-21G** level.

Table 4. Ground-State Relative Energies Computed at the AM1 and B3LYP/3-21G** Levels and HOMO and LUMO Energies (eV) at the B3LYP/3-21G** level

	E_{rel} (kcal/mol)				
adduct	AM1	B3LYP/3-21G**	E_{HOMO}	E_{LUMO}	ΔE^b
2b	0.0	0.0 (0.0)[a]	−5.85	−3.21	2.64
3b	17.1	18.7 (15.5)[a]	−5.41	−3.54	1.88
4b	21.8	23.6 (22.8)[a]	−5.85	−3.29	2.56

[a] Single point energies at B3LYP/6-31G**level are in parentheses. [b] $\Delta E = E_{LUMO} - E_{HOMO}$.

0.098 mm^{-1}, $\theta_{max} = 27.49°$, $T = 90.1$ K, 57,893 measured reflections, 14,038 independent reflections, 1123 refined parameters, GOF = 1.047, $R_1 = 0.1047$ and $wR_2 = 0.2284$ for all data; $R_1 = 0.0778$ for 10,377 independent reflections ($I > 2.0\sigma(I)$), largest difference peak and hole 1.13 and −0.72 e $Å^{-3}$, respectively.

CCDC 767620 (**2b**), 767619 (**2b** and **3b** mixed crystal), 767618 (**4b**), and 767617 (**5a**) contain the supplementary crystallographic data for this paper. These data are obtainable free of charge from The Cambridge Crystallographic Data Centre via www.ccdc.cam.ac.uk/data_request/cif.

Computational Method. Full geometry optimizations were performed at AM1; then they were reoptimized at B3LYP/3-21G**.[21] B3LYP/6-31G** single-point energies were computed using B3LYP/3-21G** optimized geometries.

Acknowledgment. This work was supported in part by a Grant-in-Aid for Scientific Research on Innovative Areas (No.

20108001, "pi-Space"), a Grant-in-Aid for Scientific Research (A) (No. 20245006). The Next Generation Super Computing Project (Nanoscience Project), Nanotechnology Support Project, and Grant-in-Aid for Scientific Research on Priority Area (Nos. 20036008, 20038007) from the Ministry of Education, Culture, Sports, Science, and Technology of Japan.

Supporting Information Available: Complete refs 8b,8g,8l, 19, and 21d; crystallographic data in CIF format; spectroscopic data; and theoretical results for the silylated fullerenes. This material is available free of charge via the Internet at http://pubs.acs.org.

JA1049719